

1
2
3
4
5
6
7
8
9
10
11
12
13
14
15
16
17
18
19
20
21
22
23
24
25
26
27
28
29
30
31
32
33
34
35
36
37
38
39
40
41
42
43

**The Seasonal Phases of an Arctic Lagoon Reveal the
Discontinuities of pH Variability and CO₂ Flux at the Air-sea
Interface**

Cale A. Miller^{1,3}, Christina Bonsell², Nathan D. McTigue², Amanda L. Kelley³

¹ Department of Evolution and Ecology, University of California Davis, Davis, CA, USA, 95616

² Marine Science Institute, The University of Texas at Austin, Port Aransas, TX, USA, 78373

³ College of Fisheries and Ocean Sciences, University of Alaska Fairbanks, Fairbanks, AK,
USA, 99775

Correspondence to: Cale A. Miller (cmill@ucdavis.edu; calemiller620@gmail.com)

Deleted: Non-linear

Deleted: Extremes

Formatted: Subscript

46

47 Abstract

48 The western Arctic Ocean, including its shelves and coastal habitats, has become a focus in
49 ocean acidification research over the past decade as the colder waters of the region and the
50 reduction of sea ice appear to promote the uptake of excess atmospheric CO₂. Due to seasonal
51 sea ice coverage, high-frequency monitoring of pH or other carbonate chemistry parameters is
52 typically limited to infrequent ship-based transects during ice-free summers. This approach has
53 failed to capture year-round nearshore carbonate chemistry dynamics which is modulated by
54 biological metabolism in response to abundant allochthonous organic matter to the narrow shelf
55 of the Beaufort Sea and adjacent regions. The coastline of the Beaufort Sea comprises a series of
56 lagoons that account for > 50 % of the land-sea interface. The lagoon ecosystems are novel
57 features that cycle between “open” and “closed” phases (i.e., ice-free, and ice covered,
58 respectively). In this study, we collected high-frequency pH, salinity, temperature, and PAR
59 measurements in association with the Beaufort Lagoon Ecosystems—~~Long Term Ecological~~
60 ~~Research~~—for an entire calendar year in Kaktovik Lagoon, Alaska, USA, capturing two open
61 water phases and one closed phase. Hourly pH variability during the open water phases are some
62 of the fastest rates reported, exceeding 0.4 units. Baseline pH varied substantially between open
63 phase 2018 and open phase 2019 ~~from ~ 7.85 to 8.05, respectively,~~ despite similar hourly rates of
64 change. Salinity-pH relationships were mixed during all three phases displaying no correlation in
65 open 2018, a negative correlation in closed 2018 – 2019, and positive correlation during open
66 2019. The high-frequency of pH variability could partially be explained by photosynthesis-
67 respiration cycles as correlation coefficients between daily average pH and PAR were 0.46 and
68 0.64 for open 2018 and open 2019 phases, respectively. The estimated annual daily average CO₂
69 efflux (~~from sea to atmosphere~~) was $5.9 \pm 19.3 \text{ mmol m}^{-2} \text{ d}^{-1}$, which is converse to the negative

Deleted: LTER

Deleted: with a difference of ~ 0.2 units

72 influx of CO₂ estimated for the coastal Beaufort Sea despite exhibiting extreme variability.
73 Considering the geomorphic differences such as depth and enclosure in Beaufort Sea lagoons,
74 further investigation is needed to assess if there are periods of the open phase in which all
75 lagoons are sources of carbon to the atmosphere, potentially offsetting the predicted sink
76 capacity of the greater Beaufort Sea.

77
78
79
80
81
82
83
84
85
86
87
88
89
90
91
92
93
94
95
96
97
98

99

100

101

102

103

104

105

106

1 Introduction

Acidification of the Arctic Ocean is predicted to proceed at a faster rate than lower latitude regions due to the increased solubility of CO₂ in colder waters, intrinsically lower carbonate ion concentration, and specific water mass mixing patterns [with deep Pacific water and surface freshwater](#) (Fabry et al., 2009; Mathis et al., 2015). The acidification phenomenon which increases the dissolved inorganic carbon to alkalinity ratio reduces the natural buffering capacity of the carbonate system via a reduction in carbonate ion concentration. These processes result in [a decrease of](#) calcium carbonate saturation state and [sea surface pH](#). It is estimated that the Canadian Basin, Beaufort Sea, and Chukchi Sea in the Arctic have experienced a 2.7 % shoaling of low [aragonite](#) saturation state ($\Omega_{arg} < 1.25$) waters from 0 – 250 m over the past 2 decades (Qi et al., 2017; Zhang et al., 2020). Future projections anticipate a continuation of this trend with sustained, perennial, undersaturation of calcium carbonate ($\Omega_{arg} < 1$) in the Beaufort and Chukchi Seas by the year 2040, which will reduce the capacity of these waters to continually take up atmospheric CO₂ (Mathis et al., 2015). The rate at which this happens will have significant implications on the current estimates of CO₂ uptake by the coastal Chukchi and Beaufort Seas (Evans et al. 2015a). Acidification of offshore Arctic waters appear to be a consequence of increasing Pacific Winter Water intrusion due to globally warming waters and an influx of excess atmospheric CO₂ caused by the disequilibrium between air and seawater PCO₂ (Qi et al., 2017). Along the nearshore regions of the Beaufort Sea, however, coastal processes predominately drive acidification such as riverine flux of freshwater, biological metabolism, sea-ice melt from warming waters, and upwelling of the Polar Marine Layer which is an important water source for Arctic lagoons ([Miller et al., 2014; Wynn et al., 2016; Harris et al., 2017; Carstensen and Duarte, 2019; Woosley and Millero, 2020](#)).

Deleted: ¶

Deleted: low

Deleted: a low

Deleted: Carstensen and Duarte, 2019; Harris et al., 2017;

Deleted: ; Wynn et al., 2016

135 The coastal margin of the Beaufort Sea consists of biologically complex, shallow (< 6 m),
136 discontinuous, estuarine lagoons that depict ~ 50 % of the coast from Nuvuk (Pt. Barrow) to
137 Demarcation Bay, Alaska, USA ([Lissauer et al., 1984](#); Dunton et al., 2006, 2012; Harris et al.,
138 2017). The North Slope region is predominately tundra, where the annual terrestrial thaw
139 comprises the majority of the freshwater outflow to the Beaufort Sea. Canada's Mackenzie River
140 is the largest source of freshwater flowing into the Beaufort Sea, ~ 300 km³ yr⁻¹ ([Stein and](#)
141 [Macdonald, 2004](#); McClelland et al., 2006); however, many smaller rivers and streams link the
142 terrestrial hydrography with the marine lagoon ecosystem characterized as geomorphic transition
143 zones (Dunton et al., 2006, 2012). Barrier islands partially obstruct Beaufort Sea coastal water
144 exchange with the lagoons, which in part are hydrographically influenced by the seasonal shifts
145 in terrestrial freshwater flux that results in highly dynamic chemical conditions (Mouillot et al.,
146 2007). Flow channels between the land, Arctic lagoons and the ocean are ephemeral, causing the
147 flow of water in and out of a lagoon to be intermittent, varying on short- and long-term time
148 scales ([Kraus et al., 2008](#); Dunton et al., 2012). These physical flow attributes result in highly
149 variable salinity and temperature that range from fresh to hypersaline (0 to >45), and -2 °C to 14
150 °C, respectively (Dunton and Schonberg, 2006; Harris et al., 2017). This variability in
151 temperature and freshwater delivery can have a dramatic effect on carbonate chemistry
152 thermodynamics and modify alkalinity and dissolved inorganic carbon (DIC). The seasonality of
153 these shallow lagoons is distinguished by two principal phase states corresponding to sea ice
154 prevalence—open and closed. The closed period during winter ice cover exhibits a non-
155 quantifiable amount of air-sea exchange due to the physical sea ice barrier. Conversely, the open,
156 ice-free summer period from late spring to early fall is marked by spring river discharge, air-sea
157 exchanges, and [storm activity](#) (McClelland et al., 2012, 2014). Episodic fluctuations in lagoon

Deleted: ; Lissauer et al., 1984

Deleted: ; Stein and Macdonald, 2004

Deleted: ; Kraus et al., 2008

Deleted: meteorological events

162 hydrography during periods of open water add to the complexity of physicochemical variability
163 as wind-driven upwelling events coupled with tidal flux can precipitate rapid changes in these
164 semi-isolated bodies of water (Lissauer et al., 1984).

165 Despite extreme variability in temperature and salinity, Arctic lagoons are home to
166 diverse fish assemblages that include diadromous, freshwater, and marine species (Robards,
167 2014; Harris et al., 2017; Tibbles, 2018), many of which serve as important subsistence fisheries
168 for Arctic communities (Griffiths et al., 1977; Craig, 1989). Arctic lagoons have relatively high
169 diversity and abundance of benthic community invertebrates, ranging from 654 to 5,353
170 individuals m⁻² with trophic linkages to birds and marine mammals (Griffiths et al., 1977,
171 Johnson et al., 2010; Dunton et al., 2012). The benthic food web relies on both autochthonous
172 microalgal production and allochthonous terrestrial organic matter (OM) inputs as carbon
173 subsidies (Harris et al., 2018). The deposition of these carbon subsidies may have implications
174 on the chemical conditions of lagoon ecosystems via enhanced remineralization during the
175 during open and closed phases. To date, hydrographic physicochemical measurements have been
176 mostly limited to the open [summer] season with few exceptions (Kinney et al., 1971; Mathews
177 and Stringer, 1984; Dunton and Schonberg, 2006; Robards, 2014). To our knowledge, only a
178 single high-frequency year-round measurement of Beaufort Sea lagoon temperature and salinity
179 exists (Harris et al., 2017), which is insufficient for understanding how these factors including
180 biological metabolism may impact carbonate system dynamics.

181 This study is the first to incorporate a high-frequency time series of salinity, temperature,
182 PAR, and pH for an entire calendar year capturing both open and closed phases of an Arctic
183 lagoon. The Kaktovik Lagoon located adjacent to Barter Island and the city of Kaktovik was
184 selected for sensor package deployment. The data collected in this study were processed in part

Deleted: Robards, 2014;

Deleted: ; Griffiths et al., 1977

Deleted: Dunton and Schonberg, 2006;

188 with those available from the Beaufort Lagoon Ecosystems (BLE) Long Term Ecological
189 Research Program (LTER) and the NOAA Earth Systems Research Laboratory (ESRL). Salinity,
190 temperature, and pH were analyzed in the time and frequency domains alongside ancillary solar
191 radiation and water depth in order to examine potential modifiers of pH. This included estimates
192 of carbon flux at the land-sea interface utilizing atmospheric PCO₂ measurements and comparing
193 those with derived seawater PCO₂ estimates. The findings of this study are presented in the
194 context of seasonal variability of oceanographic processes in an ecosystem that is part of the
195 western coastal Arctic that is experiencing climate change.

196

197 **2 Study site and methods**

198 **2.1 Kaktovik Lagoon ecosystem**

199 Kaktovik Lagoon, Alaska (70° 6' 3" N 143° 34' 52" W), serves as one of the study sites for the
200 National Science Foundation's Beaufort Lagoon Ecosystems LTER. It is one of a series of
201 coastal lagoons that fringe the Arctic National Wildlife Refuge and borders the east side of
202 Barter Island. With a maximum depth of approximately 4.4 m, Kaktovik Lagoon has two narrow
203 exchange pathways with adjacent water bodies (Dunton et al., 2012). One of the pathways
204 connects to Arey Lagoon, the other links to Jago Lagoon and to the Beaufort Sea via a channel >
205 25 m long and < 2.5 m deep (Fig. 1). Surface freshwater inputs are limited to small tundra
206 streams, although narrow inlets provide some exchange to adjacent Arey and Jago Lagoons,
207 which receive terrestrial inputs from the Hulahula/Okpilak and Jago Rivers, respectively. The
208 timing of sea ice formation varies by year but occurs between late September and October
209 becoming landfast (fastened to the coastline) in the shallow lagoons until breakup in May or June
210 (Dunton et al., 2006).

Deleted: (

Deleted:)

213
214
215
216
217
218
219
220
221
222
223
224
225
226
227
228
229
230
231
232
233
234
235

2.2 Oceanographic sampling

A benthic mooring outfitted with a SeaBird SeaFET V2 and RBR Concerto CTD++ was deployed 8 August 2018 to 11 August 2019, with sensors roughly 10 cm from the bottom in Kaktovik Lagoon (Fig. 1). Hourly measurements of pH, salinity, and temperature (from SeaFET thermistor) were recorded (UTC) throughout the deployment period. A separate, adjacent mooring consisting of a LI-COR spherical quantum sensor in-line with a LI-1000 datalogger recorded photosynthetically active radiation (PAR $\mu\text{mol photons m}^{-2} \text{ s}^{-1}$; 400-700 nm) ~30 cm from the bottom. Average PAR was integrated over three-hour time periods and recorded. In ~~August 2018, April 2019, and June 2019,~~ the site was sampled for dissolved nutrients and physicochemical (~~i.e., temperature and conductivity~~) parameters within 30 cm of water surface and within 30 cm of the bottom. Physicochemical parameters were recorded with a YSI ProDSS calibrated daily before excursions. Nutrient samples were collected with a peristaltic pump fitted with Masterflex C-flex tubing, then filtered through a Geotech 0.45 μm high-capacity polyethersulfone (PES) capsule filter connected with Masterflex-C tubing and frozen at -20 °C until analysis. Sediment was retrieved from the seafloor by a 0.1 m² van Veen grab, sampled with 50 mL push core and frozen at -20 °C until analysis. Porewater was extracted by centrifugation of defrosted sediment, then analyzed immediately. Dissolved nutrients in water and porewater [ammonia (NH₃), nitrate + nitrite (NO_x), orthophosphate (PO₄³⁻), and silica (SiO₂)] were measured at the Core Facilities Laboratory at The University of Texas Marine Science Institute in Port Aransas, Texas, on a continuous flow-analyzer Lachat Quick Chem 8500.

Deleted: August,

Deleted: ,

2.3 Seawater chemistry and pH sensor calibration

Discrete bottle samples were taken approximately 10 cm off the bottom proximal to the sensor on 17 August 2018 for SeaFET calibration, and 26 April 2019 for reference. Bottle samples were collected in duplicate and processed for total alkalinity (A_T) and pH_T (total scale). An additional A_T sample was collected on 21 June 2019. The August 2018 sample was gathered by Van Dorn bottle, where a single sampling was used to fill duplicate bottle replicates. April 2019 duplicate samples were directly collected from depth by a peristaltic pump fitted with MasterFlex C-flex tubing. All seawater samples were placed in 500 mL borosilicate bottles and fixed with 200 μ L saturated mercuric chloride and held at 4 °C until laboratory analysis.

A_T was measured with an open-cell titrator using 0.1 M hydrochloric acid titrant on a Metrohm Titrino 848 (Dickson et al., 2007: SOP 3b). Spectrophotometric pH_T measurements were made in duplicate using a Shimadzu 1800 outfitted with a cuvette temperature controller stabilizing temperature at 25 °C. The spectrophotometric pH_T was determined using *m*-cresol purple (Acros, batch # 30AXM-QN), following SOP 6b from Dickson et al. (2007). An impurity correction factor of the *m*-cresol reagent was used to adjust the final measured pH_T value (Douglas and Byrne, 2017). All *benchtop* salinity measurements were conducted with a YSI 3100 conductivity meter. Certified Reference Material of seawater (CRM: Batch 172, A.G., Dickson, Scripps Institute of Oceanography) was used to calculate the A_T and *m*-cresol dye uncertainty. Calibration and reference *in situ* pH_T samples were derived using the Matlab version of CO2SYS (van Heuven et al., 2011) with input parameters salinity, temperature (*from thermistor*), pH_T , and A_T using *carbonic acid* dissociation constants from Lueker et al. (2000), *the bisulfate dissociation constant of* Dickson et al. (1990), and *the boron constant from* Uppström (1974). *Given the broad spectrum of salinity values and low temperatures in this study, potential*

Deleted: -

Formatted: Font: Not Italic, Not Superscript/ Subscript

Commented [CMI]: L. 256 Reviewer 1

262 uncertainties may be present and difficult to quantify. Dinauer and Mucci (2017) found that
 263 dissociation constants derived by Cai and Wang (1998) were best applied to low salinity waters
 264 when estimating PCO₂, whereas Lueker constants overestimated values by $\lesssim 40 \mu\text{atm}$.
 265 Conversely, Sulpis et al. (2020) found that at low temperatures ($< 10^\circ\text{C}$) Lueker constants
 266 underestimated K₁* and K₂* constants resulting in PCO₂ values $\sim 20 \mu\text{atm}$ lower. Given the
 267 mostly compensatory nature of salinity and temperature, the Lueker constants provide a medium
 268 estimate for the purposes of this study when calibrating across the entire time series.

Formatted: Subscript

Deleted: ¶

Formatted: Subscript

Formatted: Subscript

Formatted: Subscript

269 A SeaFET conditioning period of 9 d was conceded from deployment on 8 August 2018
 270 to 17 August 2018 when the calibration sample was collected. A single-point calibration was
 271 applied following previously established best practices (Bresnahan et al., 2014; Miller et al.,
 272 2018). New calibration coefficients for the SeaFET were then applied and used to calculate pH_T
 273 from the internal ISFET electrode for the entire dataset (Martz et al., 2010). The single reference
 274 sample taken on 26 April 2019 was used to compare against SeaFET measured pH_T as a check
 275 for sensor drift and robustness of calibration.

276

277 2.3.1 Uncertainty estimate

278 The reliability and accuracy of SeaFET sensors is dependent on estimating the total uncertainty
 279 attributable to an individual sensor's behavior and operator usage (Bresnahan et al., 2014; Rivest
 280 et al., 2016; McLaughlin et al., 2017; Gonski et al., 2018; Miller et al., 2018). A previous method
 281 for calculating the total uncertainty associated with SeaFET function has been previously
 282 proposed and was applied to this study (Miller and Kelley, *in press*). Briefly, a propagated
 283 uncertainty Eq. (1) was derived by adding in quadrature the standard deviation of analytical
 284 replicates measuring CRM pH_T spectrophotometrically, a titrator uncertainty comparing

Deleted: McLaughlin et al., 2017;

Deleted: ; Rivest et al., 2016

Deleted: 2020

Deleted: in review

measured and known A_T from CRM, the standard deviation of discrete pH_T bottle replicates, and the uncertainty associated with CO2SYS dissociation constants using the Matlab errors function described in Orr et al. (2018). An additional salinity uncertainty not described in Miller and Kelley (*in press*) was added to account for the discrepancy between benchtop salinity measurements and *in situ* readings found in this study (Table S1). The final equation reads:

$$Q = \sqrt{\sigma_{m-cresol}^2 + \sigma_{bottle\ replicates}^2 + \sigma_{CO2SYS\ constants}^2 + \sigma_{salinity}^2 + AN_{titrator}^2} \quad (1)$$

where Q is the propagated uncertainty, AN is the anomaly between measured and known A_T , and σ is the standard deviation of all of the uncertainty input parameters in pH units (see Miller and Kelley 2020 *in press*). From this point, the total uncertainty was calculated by taking the average of the propagated uncertainties for the calibration sample, reference sample, and bottle anomaly (Table 1). This propagated uncertainty was then applied to the entire pH_T time series.

301

302 2.4 Ancillary data acquisition

The Beaufort Lagoon Ecosystems LTER data on current velocity, water depth, and underwater PAR was accessed through the Environmental Data Initiative portal. Current velocity was used as a proxy to determine the open and closed (i.e., ice covered or ice-free) seasons for the lagoon. A velocity consistently below 2 cm s^{-1} for a period $>10\text{ h}$ was designated as a threshold for the two phases (Fig. S1). Water depth derived from the pressure sensor was interpreted as tidal variation, where consistent frequencies in depth changes were applied for analysis (see 2.5). Instantaneous PAR measurements were used to determine daily average values for time series analysis.

311

312 2.5 Frequency Analysis

Deleted: 2020 in review

Deleted: ²

Deleted: in review

316 A power spectral density (PSD) analysis of pH_T, temperature, salinity, and tide was performed
 317 using the *pwelch* function in Matlab (v2020a) to determine the magnitude of variation at a given
 318 frequency during each phase: open 2018, closed 2018 – 2019, and open 2019. This function
 319 processes data as samples s⁻¹, so for 24 measurements in a day, a sampling rate of 2.78 x 10⁻⁴ was
 320 applied with a frequency of d⁻¹. A Hamming window was used for sidelobe attenuation (*i.e.*,
 321 *adjusting width of main peak*) of the analyses and the mean value for each parameter was
 322 subtracted in order to examine only the variation around the mean. Residual noise around a
 323 frequency of *zero* was muted by applying a Butterworth high-pass filter with an order of *three*,
 324 and cut off frequency at 1.0 x 10⁻⁵. If two of the analyzed variables exhibit the same predominant
 325 frequency, then their variation is assumed to be correlated regardless of direction and magnitude.
 326 Previous PSD analyses with similar parameters have been shown to be considerably noisy below
 327 ~ 50 dB Hz⁻¹, thus making this value a cutoff threshold for the purposes of this study (Miller and
 328 Kelley *in press*). *Frequency peaks corresponding to 1 and 2 d⁻¹ are likely a response to the*
 329 *semidiurnal tidal cycle, while a frequency of 3 d⁻¹ to daily changes in PAR.*

Formatted: Line spacing: Double

Deleted: 0

Deleted: 3

Deleted: ate

Commented [CM2]: Reviewer 1 D

Deleted: in review

Formatted: Superscript

Formatted: Superscript

331

332 2.6 A_T, PCO₂, and flux calculations

333 Salinity recorded by the RBR Concerto CTD++ were filtered for invalid measurements taken
 334 over the year-long time series. *Erroneous data* (below the freezing point of water *as defined by*
 335 *the temperature-salinity relationship*) were removed, and a linear interpolation was performed to
 336 replace the missing values (Fig. S2). Two linear regression analyses were performed to estimate
 337 A_T, one with measured *in situ* salinity and the other with benchtop recorded values. Each analysis
 338 was constructed with the three discrete A_T samples collected on 17 August 2018, 26 April 2019,

Deleted: Measurements identified

Deleted: as

Deleted: due to the

and 21 June 2019 (Table S1), where A_T is the dependent variable and salinity the independent. Benchtop values were considered to be more robust as the YSI 3100 Conductivity meter was calibrated to the manufacturer's specification, while the CTD++ was factory calibrated. For this reason, the regression from the benchtop salinity measurements were considered to be the primary hourly A_T values; however, both A_T estimates from benchtop (slope = 59.71, $R^2 = 0.968$) and *in situ* (slope = 48.38, $R^2 = 0.998$) salinity were used as input parameters along with measured pH_T to calculate hourly PCO_2 values (Fig. S3) using CO2SYS (see above for constants applied).

Atmospheric hourly PCO_2 averages were collected from the NOAA ESRL station at Barrow (Utqiagvik), Alaska, USA (Thoning et al., 2020), and wind speed was acquired from automated airport weather observations from the Barter Island Airport. Using these data, a CO_2 air-sea flux for open phases 2018 and 2019 was calculated following the bulk transfer method with a gas transfer velocity constant k as modified by the Schmidt number (i.e., ratio of kinematic viscosity of water to gas diffusivity), which is a function of temperature and salinity. The bulk flux equation in Wanninkhof (2014) was used for the estimate:

$$F_{bulk} = 0.251 U^2 (Sc/660)^{-0.5} K_0 (PCO_{2w} - PCO_{2a}) \quad (2)$$

where U is wind speed in $m s^{-1}$, $Sc/660$ is the Schmidt number calculated using the coefficients from the 4th order polynomial in Wanninkhof (2014: Table 1), K_0 is temperature and salinity dependent solubility of CO_2 in $mol L^{-1} atm^{-1}$ calculated following the model presented in Wanninkhof (2014: Table 2), and PCO_2 is the partial pressure of CO_2 in water (w) and air (a) in atm. The uncertainty applied to the flux estimates are defined as the flux potential given the

Formatted: Superscript

Formatted: Superscript

Deleted: <

Deleted: >

Deleted: Schmidt

Commented [CM3]: Rveiewer 2 question 2

372 broad spectrum of salinity and how it affects the gas transfer velocity, and the A_T estimates
 373 derived from the *in situ* and benchtop measured salinity values. The flux potential uncertainty
 374 was chosen because the values estimated were equal to or more extreme than those identified
 375 from the total uncertainty of the pH measurements, if the total pH uncertainty was applied as a
 376 proportion to the A_T derived values. Since the Schmidt number is a function of temperature and
 377 salinity, a freshwater value was derived using the f_w coefficients presented in Wanninkhof
 378 (2014). This estimate provided a more conservative flux and was, therefore, presented as the
 379 lower bound uncertainty in the estimate. The upper bound uncertainty of the flux estimate was
 380 calculated by applying the PCO₂ values into Eq. (2) derived from the salinity_{in situ}- A_T regression.
 381 These values resulted in a larger flux estimate, which is why they were set as the upper bound.
 382 Both the lower and upper bounds were then applied as the estimated total uncertainty, flux
 383 potential.

384

385 **2.7. Statistical methods and data manipulation of pH covariates**
 386 Relationships between pH_T and salinity were correlated by applying a 2nd order polynomial fit
 387 for the closed 2018 – 2019 phase and open 2019 phase with salinity as the explanatory variable.
 388 This included detrending pH_T and reexamining relationships with salinity for open phase 2018
 389 where no correlation was found. Linear regression between temperature and pH_T was performed
 390 for each phase of the time series. pH_T and PAR hourly variations were collapsed by calculating
 391 the daily averages for both parameters. The average daily values for pH_T open 2018 and 2019
 392 were then detrended to remove correlations with salinity and any potential covariates not
 393 captured in this study. A Pearson's correlation coefficient was then derived between the
 394 detrended pH_T daily averages and PAR daily averages for open 2018 and open 2019.

Formatted: Font: Italic, Subscript

Formatted: Font: Italic

Deleted: Schmidt

Formatted: Font: Italic, Subscript

Deleted: (

Deleted: ,

Deleted: for the

Deleted: estimate

Deleted:

Deleted: 6

Deleted: applications

Deleted: quadratic

Formatted: Superscript

Commented [CM4]: Reviewer 1 A

Deleted: No

Deleted: existed for open 2018

Formatted: Font: 12 pt

Deleted:

Commented [CM5]: Reviewer 2 line 330

407

408 3 Results

409 3.1 Time series

410 The year-long time series of pH_T , temperature, and salinity was recorded from 17 August 2018 to
411 11 Aug 2019 (Fig. 2). Based on the current velocity threshold of 2 cm s^{-1} as a proxy for sea ice
412 cover, the 2018 open phase transitioned to a closed phase on 8 October 2018 which terminated
413 on 22 June 2019 as the 2019 open phase began (Fig. S1). Both calibration and reference samples
414 that were collected in duplicate have a fairly high standard deviation at 0.099 and 0.088,
415 respectively. The large deviation between duplicate samples was the greatest source of
416 uncertainty (see Eq. 1) for the entire pH_T time series, which shows the total uncertainty shaded in
417 grey (Fig. 2a) and found in (Table 1). Invalid salinity values were $\sim 6 \%$ of the entire time series,
418 with the greatest proportion of interpolated values concentrated in the closed phase (Fig. 2c).

419 In the open phase of 2018 pH_T values were highly variable in August ranging from 7.66
420 to 8.40, which was the highest pH_T recorded for the entire calendar year (Fig. 3a). An upward
421 trend in pH_T began on 21 August and steadily increased indicating a continued accuracy of the
422 internal ISFET at low salinity. The low episodic salinity event when values were < 9 occurred
423 from 23 August to 27 August 2018, which was after the sporadic variability in pH_T days earlier
424 (Fig. 3). From September until freeze-up on 8 October, pH_T variability was low with the 7-d
425 running average maintaining at ~ 8.10 and fluctuating between 8.07 to 8.18. Temperature
426 followed a steady decrease with a negative slope of 0.12 (Fig. 3b). Salinity rose steadily although
427 instances of large episodic events were present, and in one instance on 1 September, salinity
428 increased from 12.9 to 23.1 in an 8 h period (Fig. 3c).

Deleted: and

Deleted: < 0.1 units

431 During the closed phase when Kaktovik Lagoon first became ice-covered, pH_T continued
 432 to remain somewhat invariant around ~ 8.10 as it did during the previous two open-water months
 433 (Fig. 4a). Approximately 2 weeks into the closed phase, pH_T began to steadily decrease until
 434 stabilizing in the beginning of January at ~ 7.71. pH_T varied between 7.55 and 7.85 from this
 435 point until April when another negative trend culminated at a low of 7.48. Late May saw pH_T
 436 levels increase until phase transition on 22 June 2019. Temperature stayed below -1 °C until late
 437 May when it began to increase concomitantly with pH_T approaching 0 °C (Fig. 4b). Salinity
 438 values increased from 31 at the start of ice cover reaching a maximum of 39.2 in April (Fig. 4c).

439 Open phase 2019 saw extreme pH_T variability beginning 21 June to 11 August 2019 with
 440 the rate of hourly change reaching as high as 0.467 units from 7.78 to 8.26 in mid-July (Fig. 5a).
 441 During the first portion of this phase, the pH_T running average was consistent at ~ 8.05 with
 442 minimal variability. Episodic fluctuations caused pH_T values to reach as high as 8.33. A negative
 443 trend began in late July shifting the running average to ~ 7.79, which was lower than the 7.94
 444 running average in August 2018. Temperature increased rapidly during the first 2 weeks
 445 following breakup and then remained stable around 10 °C (Fig. 5b). Salinity decreased steadily
 446 for the first month after breakup followed by large episodic freshening events in late July (Fig.
 447 5c); these were similar to the events seen in the open phase of 2018.

448 Correlations between salinity and pH_T were inconsistent and varied by phase. Open phase
 449 2018 pH_T was not correlated with salinity which ranged from 5 to 30, while pH_T was
 450 predominantly steady shifting only ± 0.1 units around 8.0 (Fig. 6a). A weak negative correlation
 451 between temperature and pH_T existed ($R^2 = 0.19$), however removing this trend did not result in
 452 changes between salinity and pH_T. The maximum range of pH_T during this period was confined
 453 to salinity values between 11.5 to 12.5. During the closed phase, pH_T correlated well with

Deleted: and shifting only ± 0.05 units.

Deleted: ~ 0.2 units

Deleted:

Deleted: -

Formatted: Line spacing: Double

Commented [CM6]: Reviewer 1 A

Formatted: Font: 12 pt

Formatted: Font: 12 pt

458 salinity, which ranged from ~ 30 to 40 (Fig. 6b). An inverse relationship between salinity and
 459 pH_T was present during this phase with an R^2 of 0.69. The opposite pattern was observed during
 460 open phase 2019, however, where salinity and pH_T were positively correlated with an R^2 of 0.66
 461 (Fig. 6c). Overall, the temperature relationships with salinity were due to seasonal timing rather
 462 than intrusion of water mass or mixing. Smoothed data as 7-d running averages between pH_T and
 463 temperature, and pH_T and salinity, did not reveal any significant correlations.

Deleted: in

Deleted: T

Commented [CM7]: Reviewer 1 A

466 3.2 Frequency of pH variability

467 The PSD of pH_T during open phase 2018 and closed phase 2018 – 2019 were weak with the
 468 majority of peaks around any given frequency falling under 50 dB Hz⁻¹ (Fig. 7a and b). Peaks of
 469 pH_T during open 2018 did not correspond with any regular frequencies across temperature,
 470 salinity (Fig. 7) or tide (Fig. S4), which only displayed regular peaks at a frequency of 1 and 2 d⁻¹.
 471 Consistent variability of pH_T during the closed phase was negligible but had a maximum
 472 magnitude at a frequency of 0.39 which corresponded to a peak observed with temperature (Fig.
 473 7b and e). Open phase 2019 had a multitude of peaks with frequencies ranging from 0.5 to 7.5 d⁻¹,
 474 however most fell under 50 dB Hz⁻¹ (Fig. 7c). The highest magnitude of pH_T corresponded
 475 well with tide at ~ 1 d⁻¹ (Fig. 7c and Fig. S4c). Salinity also displayed a strong peak at 1 d⁻¹ (Fig.
 476 7i), sharing this frequency of variability with pH_T and tide.

Deleted: 3

Deleted: 3

478 3.3 pH response to PAR

479 Open phase 2018 and open phase 2019 daily average pH_T was compared against instantaneous
 480 underwater PAR levels recorded for both phases (Fig. 8). Open phase 2018 PAR levels were

consistently lower compared to open phase 2019 as a result of the time of year the two phases were observed (Fig. 8). The detrended daily average pH_T correlated well with daily average PAR with a Pearson's correlation coefficient of 0.469 (p -value = 0.005). In early August 2018, PAR levels $> 5 \mu\text{mol photons m}^{-2} \text{s}^{-1}$ were not representative of, high, daily average pH_T . This was a deviation from the general trend of the open 2018 phase in which daily average pH_T was positively correlated with instantaneous PAR (Fig. 8a). In late August and September, high values of daily average $pH_T > 8.20$ coincided with spikes in instantaneous PAR that exceeded $10 \mu\text{mol photons m}^{-2} \text{s}^{-1}$ (Fig. 8a).

Open phase 2019 daily average pH_T was overall more variable than open phase 2018 with values from 7.66 in early August to 8.09 in late June (Fig.8b). The detrended daily average pH_T had a more robust correlation with daily average underwater PAR than in 2018 with a Pearson's correlation of 0.643 (p -value < 0.001). The highest PAR values were recorded in mid-July; however, this did not correlate with the highest daily average pH_T which was observed in late June. Consistent high values of PAR in mid-July corresponded to relatively flat daily average pH_T (Fig. 8b). A reduction in instantaneous PAR to values below $15 \mu\text{mol photons m}^{-2} \text{s}^{-1}$ in late July was linked with a gradual decrease in daily average pH_T . During this 11-d period, daily average pH_T dropped from 8.06 to 7.71, and only began to increase again when instantaneous PAR exceeded $25 \mu\text{mol photons m}^{-2} \text{s}^{-1}$ for consecutive days.

3.4 Flux Estimation

Carbon flux estimates for open phase 2018 and open phase 2019 showed dramatically different results with 13 instances exceeding a flux $> 10 \mu\text{mol CO}_2 \text{ m}^{-2} \text{ min}^{-1}$ compared to 302 instances in open phase 2019 (Fig. 9)—where $10 \mu\text{mol CO}_2 \text{ m}^{-2} \text{ min}^{-1}$ is \approx to $2 \text{ mmol CO}_2 \text{ m}^{-2} \text{ d}^{-1}$ which is the

Deleted: 0

509 equivalent magnitude, but opposite of the estimated annual mean sea-air flux for the coastal
510 Beaufort Sea, $-2 \text{ mmol CO}_2 \text{ m}^{-2} \text{ d}^{-1}$ (Evans et al, 2015a). The episodic events of flux from the
511 atmosphere into seawater was greater in 2018 with 21 instances $< -10 \text{ } \mu\text{mol CO}_2 \text{ m}^{-2} \text{ min}^{-1}$
512 compared to a single instance in 2019. The maximum lower bound ~~flux potential~~ for open phase
513 2018 was estimated at $2.23 \text{ } \mu\text{mol CO}_2 \text{ m}^{-2} \text{ min}^{-1}$ whereas the upper bound was $10.67 \text{ } \mu\text{mol CO}_2$
514 $\text{m}^{-2} \text{ min}^{-1}$ (Fig. 9a). Overall, wind speed correlated poorly with CO_2 flux in 2018 ($R^2 = 0.13$). The
515 highest frequency of robust wind speeds occurred in October but resulted in only a minor
516 atmospheric flux into seawater as the majority of values were between 2 and $-5 \text{ } \mu\text{mol CO}_2 \text{ m}^{-2}$
517 min^{-1} (Fig. 9a).

518 Open phase 2019 had an estimated CO_2 flux as high as $105 \text{ } \mu\text{mol CO}_2 \text{ m}^{-2} \text{ min}^{-1}$, which
519 occurred in early August (Fig. 9b). Over a 5.6 d period in late July, CO_2 flux was $> 10 \text{ } \mu\text{mol CO}_2$
520 $\text{m}^{-2} \text{ min}^{-1}$ for more than 90 % of the time reaching a high of $78 \text{ } \mu\text{mol CO}_2 \text{ m}^{-2} \text{ min}^{-1}$. The
521 maximum lower bound uncertainty ~~potential flux~~ estimate for open phase 2019 was $5.5 \text{ } \mu\text{mol}$
522 $\text{CO}_2 \text{ m}^{-2} \text{ min}^{-1}$ with an upper bound of $8.56 \text{ } \mu\text{mol CO}_2 \text{ m}^{-2} \text{ min}^{-1}$. Wind speed was found to be
523 significantly correlated with CO_2 flux ($p\text{-value} < 0.0001$, $R^2 = 0.53$) in 2019 and, thus, cogently
524 different from open phase 2018.

525

526 4 Discussion

527 Kaktovik Lagoon was an ideal location for a year-long deployment to capture the three phases
528 (i.e., open 2018, closed 2018 – 2019, and open 2019) of environmental conditions in the coastal
529 Arctic. The study site displayed annual pH variability in the context of a unique lagoon where
530 geographical and physical features of this site represent a semi-closed system with narrow
531 passages to the sea and only small tundra stream inputs. The stochastic events of pH captured in

Deleted: uncertainty

Deleted: uncertainty

534 this system are some of the most dramatic hourly pH rates of change recorded to date (Hofmann
535 et al.; 2011; Kapsenberg et al., 2015; Takeshita et al., 2015; Kapsenberg and Hofmann, 2016;
536 Cyronak et al., 2020). These findings represent a system that is often in tenuous equilibrium
537 resulting in dramatic fluctuations of CO₂ outgassing and differing magnitudes of pH sensitivity
538 to temperature and salinity. The extreme nature of these habitats displays the resilience of the
539 micro and macro faunal community that undoubtedly modify seawater pH via biological
540 processes. While this study was able to capture physical and chemical conditions of the lagoon,
541 future work should be directed toward understanding how community organization in the lagoon
542 ecosystem affect pH variability.

Deleted: Cyronak et al., 2020;

Deleted: Kapsenberg and Hofmann, 2016;

544 4.1 Kaktovik Lagoon and pH-salinity relationship

545 A crucial finding from this year-long time series was the disparity between the pH_T-salinity
546 relationship during the open 2018, closed 2018 – 2019, and open 2019 phases. Sequentially
547 through the time series, the pH_T-salinity relationship was non-existent, negatively correlated, and
548 positively correlated, indicating that multiple processes drive pH variability at differing
549 magnitudes at a seasonal-phase resolution. Given the myriad processes such as temperature-
550 salinity relationships with carbonate chemistry, current- and wind-driven flux between the
551 sediment-water interface and the air-sea interface, as well as photosynthesis and respiration
552 cycles (Zeebe and Wolf-Gladrow, 2001; Hagens et al., 2014; Carstensen and Duarte, 2019;
553 Rassmann et al., 2020), it is unsurprising that salinity was observed as only a moderate and
554 intermittent driver of pH_T variability in Kaktovik Lagoon. This is despite the multitude of
555 salinity changes that shift in time due to the discharge from rivers and tundra streams, seasonal
556 ice-formation and breakup, and water column stratification, all which would be expected to

Deleted: Hagens et al., 2014;

Deleted: ; Zeebe and Wolf-Gladrow, 2001

Deleted:

562 fluctuate pH predictably. The features intrinsic to Kaktovik Lagoon are likely important factors
563 responsible for the degree of pH_T-salinity interdependence and provide a lens that elucidates pH_T
564 altering processes that are less germane to physical oceanographic open-ocean mechanisms such
565 as temperature and salinity.

566 The characteristics of the Beaufort Sea lagoon ecosystems are unique features of the
567 coastline and exist as an interface between terrestrial inputs and seawater with each lagoon
568 varying in its connectivity to the Beaufort and freshwater sources. These lagoons temporarily
569 trap large amounts of allochthonous particulate organic carbon—which is expected to increase
570 with warming temperatures—and sediment as river and stream discharge are temporarily
571 mismatched between spring freshet and ice-covered margins (Dunton et al., 2006; Schreiner et
572 al., 2013). The lagoons adjacent to Kaktovik (Arey and Jago) are likely to be more exogenously
573 influenced due to greater connectivity to the Beaufort Sea, and the Okpilak, Hulahula, and Jago
574 Rivers. Thus, the modification of pH_T within Kaktovik Lagoon provides a baseline that is likely
575 dissimilar to adjacent lagoons providing an in-depth examination of the internal processes of a
576 “closed system” such as biological metabolism and sediment flux that can drive seasonal pH
577 variability and explain the annual shifts in moderate salinity dependence.

578 In the open phase of 2018, instances of pH_T values and the 7-d running average were
579 observed to be > 8.05 despite the striking range of salinity from 5 to 30. This included an event
580 that modulated salinity from 13 to 23 over an 8 h period, which was correlated with high NW
581 winds at ~ 20 m s⁻¹. This suggests that higher salinity waters from the adjacent Arey Lagoon
582 connecting the Beaufort Sea may have mixed into the bottom waters where the pH sensor was
583 located. The stability of salinity toward the new higher values indicates the validity of this data.

584 Open phase 2019 had a narrower range of salinity which correlated robustly with pH_T as values

Deleted: 5

Deleted: Further, the salinity range in open phase 2018 tested the limits of the ISFET sensor which had not been tested for stability below a salinity of 9 (Gonski et al., 2018), but appeared stable here.

590 above 8.0 were only observed when salinity was > 25 . While the interdependence between pH_T
 591 and salinity can be variable in nearshore systems (Carstensen and Duarte, 2019), the degree to
 592 which pH_T remained stable across a range of salinity in open 2018 is notable. Similarly, a recent
 593 study in Stefansson Sound (~ 160 km west of Kaktovik Lagoon) found that salinity-dependent
 594 nearshore pH_T varied by year, however, the range of salinity was more attenuated than in
 595 Kaktovik (Muth et al. 2020 *in review*). The difference in season between open phase 2018 (fall)
 596 and open phase 2019 (summer) could explain some of relational trends between pH_T and salinity.
 597 In the fall, storm activity and an abating thermocline can lead to greater vertical mixing,
 598 however, the wind data suggest that the incongruity between years was modest. Conversely, the
 599 summer breakup is associated with warm temperatures and enhanced freshwater input from ice-
 600 melt that can decrease pH. While these factors should be addressed in future studies, the pH
 601 trends presented here suggest that in the beginning of August both phases appear to have
 602 diverging patterns indicating yearly differences rather than predictable seasonal shifts.

603 The disparity between the salinity- pH_T correlation between the open 2018 and open 2019
 604 phases was observable in the frequency response of variability. In open phase 2018, the PSD of
 605 pH_T was low and mostly incongruent with the frequency response of salinity. This was not the
 606 case in open phase 2019 where the highest PSD was recorded at the same frequency (1.03 d^{-1}) as
 607 salinity, which was slightly offset from the PSD peak in tidal frequency at 0.98 d^{-1} . These
 608 associations suggest that events driving low salinity such as stream runoff were likely too
 609 irregular, or too low of flux, relative to the weak but consistent tidal signal driving open ocean
 610 exchange. This also corresponds to the lower range of salinity observed in open phase 2019 than
 611 in open phase 2018.

Commented [CM8]: Reviewer 2 comment 3

Formatted: Subscript

613 4.2 High-frequency pH in Arctic and Subarctic

614 Interannual variability of pH_T between open phase 2018 and open phase 2019 is not dependent
615 on a single driving factor, including time of season. In the 2018 open phase pH_T was consistently
616 high during a period when daylength was shortening and temperatures were falling. The
617 increasing trend of consistently high pH_T continued into the closed phase. Conversely, August
618 2019 pH_T had a running average that was ~ 0.2 units lower than 2018 and continued a downward
619 trend until the end of the time series. Similar findings have shown significantly different
620 interannual variability in pH along the Arctic coast that exceeded the running average difference
621 of ~ 0.2 observed in Kaktovik Lagoon by double (Muth et al. *in review*). This seasonally shifting
622 dependence of pH_T on salinity has implications for carbonate chemistry dynamics and how pH_T
623 is modified. Freshwater input from rivers have been shown to increase dissolved inorganic
624 carbon and lower A_T which can decouple the linear relationships between calcium carbonate
625 saturation state, PCO_2 , and pH ([Salisbury et al., 2008](#); Cai, 2011; Hales et al., 2016). Glacial ice-
626 melt in subarctic waters, however, is unique in that its profile is low in PCO_2 and A_T (Evans et
627 al., 2014). Both modes of freshwater carbonate chemistry decoupling may be present in
628 Kaktovik, but evidence here suggests that salinity is a non-reliable indicator of these decoupling
629 mechanisms as pH_T values can exist across a wide range of salinity and even lack relationship
630 during open phases.

631 Open phase 2019 displayed highly variable pH_T relative to open phase 2018 with an
632 inconsistent frequency of variability. In the subarctic waters off Alaska's south-central coast,
633 Jakolof Bay had a consistent seasonal trend in pH_T variability with hourly rates of change as high
634 as 0.18 ~~from ~ 7.981 to 7.801~~ (Miller and Kelley 2020, *in press*). While these rates of hourly
635 change are considered high (Hofmann et al., 2011), both open phases in Kaktovik were more

Deleted: ; Salisbury et al., 2008

Deleted: in review

638 than double that (0.401 and 0.467 from 7.655 – 8.056 and 7.789 – 8.255, respectively) of Jakolof
639 Bay. These extreme rates of change in Kaktovik can be partially explained by the photosynthetic
640 and respiratory activity within the lagoon.

Deleted: (0.401 and 0.467

641

642 4.3 PAR and pH

643 This study found robust correlations between underwater PAR and daily average pH_T. The
644 episodic nature of pH_T variability in Kaktovik Lagoon was more prevalent during periods of high
645 underwater PAR indicative of coupled diurnal photosynthesis-respiration cycles. Consistent
646 levels of PAR appeared to be associated with sustained daily average pH_T while drops in PAR
647 lowered the overall baseline pH_T. The rapid response of baseline pH_T to PAR highlights the
648 tenuous balance between the biological processes that drive pH_T modification. This phenomenon
649 is counter to what was observed in the subarctic macroalgal-dominated waters of Jakolof Bay
650 where the system maintained net autotrophy for a period > 60 days (Miller and Kelley, *in press*).

Deleted: in review

651 Possible explanations for the precarity of a dominant autotrophic or heterotrophic system may be
652 due to the shallow nature of the lagoon and frequent homogeneity of the water column. In the
653 shallow waters of the lagoon, high winds easily resuspend organic material, enhance respiration,
654 and increase light attenuation (Capuzzo et al., 2015; Moriarty et al., 2018). Thus, small decreases
655 in underwater PAR can lead to net heterotrophy. This supports the sediment “food bank”
656 hypothesis as continuous primary production is not needed to sustain heterotrophic activity, since
657 stored, labile, benthic OM can accumulate in shallow environments fueling respiration (Mincks
658 et al., 2005; Harris et al., 2018). A “bank” of OM could explain why high levels of PAR led to a
659 sustained pH_T, and any instantaneous drop in PAR was immediately followed a decrease in daily
660 average pH_T. This would suggest that high levels of PAR are only able to offset high rates of

Deleted: ; Mincks et al., 2005

Deleted:

665 heterotrophy which are sustained by the seasonal accumulation of carbon subsidies from
 666 autochthonous ice algae, phytoplankton, and influx of OM from terrestrial sources—which are
 667 likely to vary annual.

668

669 4.4 Sea ice effects on carbonate chemistry

670 A unique feature of ice covered Arctic coastal waters is the negative relationship between pH_T
 671 and salinity, which was observed here and in previous studies ([Nomura et al., 2006](#); [Miller et al.,](#)
 672 2011; [Fransson et al., 2013](#); Muth et al., *in review*). In the open ocean, salinity is positively
 673 correlated with A_T as higher salinity increases the difference between conservative cations to
 674 anions. Furthermore, A_T positively correlates with pH, and a higher A_T is associated with a
 675 higher buffering capacity. The formation of sea ice, however, induces cryoconcentration of DIC
 676 and A_T via active rejection of HCO₃⁻ during freezing and exclusion of other ions, [lowering pH](#)
 677 and creating high salinity brine drainage ([Miller et al., 2011](#); [Fransson et al., 2013](#); [Hare et al.,](#)
 678 2013). The immediate effect of high DIC concentration can lead to the precipitation of CaCO₃ in
 679 the form of ikaite (a polymorph of CaCO₃·6H₂O) along the bottom of bulk ice formation
 680 generating CO₂ as a product of the reaction and leading to [greater](#) decreases in pH ([Rysgaard et](#)
 681 [al., 2012](#); [Fransson et al., 2013](#); [Hare et al., 2013](#)). In addition, the extreme salinity and
 682 temperature in winter affect carbonate chemistry by modulating solubility, where an increase in
 683 salinity decreases CO₂ solubility, and colder temperatures increase CO₂ solubility. These salinity
 684 and temperature conditions result in a volatile thermodynamic stability of CO₂ where salinity
 685 effects outweigh temperature effects and can facilitate a degassing of CO₂ ([Papadimitriou et al.,](#)
 686 2004).

Deleted: Fransson et al., 2013;

Deleted: ; Nomura et al., 2006

Formatted: Font: Italic, Subscript

Deleted: ; Miller et al., 2011

Commented [CM9]: Reviewer 2 L 561-563

Deleted: a

Deleted: ; Rysgaard et al., 2012

692 The continually decreasing pH_T observed in this study suggests that these carbon
 693 concentrating corollaries of sea ice formation may be in effect and contribute to the negative
 694 relationship observed between pH_T and salinity. That is, if there is no outgassing of CO_2 , the
 695 relative increase in DIC and concomitant decrease in pH will be equal to that of salinity. During
 696 ice coverage, the running average of pH_T decreased from 7.93 in the beginning of November, to
 697 7.56 in late April, and mirrors the under-ice salinity trend. This decrease is nearly identical to the
 698 0.4 pH drop (~ 8.15 to 7.75) observed in the upper 2 m below the ice in Amundsen Gulf from the
 699 November to April period (Fransson et al., 2013). While this phenomenon could partially explain
 700 the general decreasing trend between pH_T and salinity, it would be remiss to state that this
 701 negative correlation is entirely driven by cryoconcentration and ikaite formation. Assuming the
 702 A_T -salinity regression calculated here is similar to a DIC-salinity correlation from
 703 cryoconcentration, the decrease in pH_T would not be great enough to explain the observations in
 704 the lagoon. While ikaite formation may be present, and further decreasing pH, the driving factor
 705 to bring the A_T :DIC ratio below 1 [which would be needed to see $\text{pH} \sim 7.55$] is likely the
 706 accumulation of respired CO_2 occurring tangentially with salinity decrease. Following a general
 707 stoichiometric relationship between N and C to be 16:106, and assuming trivial efflux of N from
 708 the sediment, the change in surface NH_4^+ from August 2018 to April 2019 would be equal to a
 709 $130 \mu\text{mol kg}^{-1}$ increase in DIC over this period (Table S1) sufficiently decreasing the A_T :DIC
 710 ratio below 1. We note that the PO_4^{3-} values are a bit anomalous, but these concentrations depend
 711 on the N:P ratio in the remineralized OM and flux of solutes from the sediment.

713 4.5 Under ice variability in pH

Deleted: o

Commented [CM10]: Reviewer 2 L572-582

Formatted: Font: Italic, Subscript

Formatted: Font: Not Italic

Formatted: Subscript

Formatted: Font: Not Italic

Formatted: Subscript

Formatted: Font: (Default) Times New Roman

Formatted: Subscript

Formatted: Superscript

Formatted: Font: (Default) Times New Roman

Formatted: Font: (Default) Times New Roman

Formatted: Font: (Default) Times New Roman

Formatted: Font: (Default) Times New Roman

Formatted: Font: (Default) Times New Roman, Superscript

Formatted: Font: (Default) Times New Roman

Formatted: Font: (Default) Times New Roman

Formatted: Font: (Default) Times New Roman

Formatted: Font: (Default) Times New Roman, Subscript

Formatted: Font: (Default) Times New Roman

Formatted: Font: (Default) Times New Roman

Formatted: Font: (Default) Times New Roman

Formatted: Font: (Default) Times New Roman

Deleted: What is more likely is that cryoconcentration is occurring in tangent with accumulated aerobic respiration byproducts overtime, and the high frequency of pH_T variability is the result of biological and thermodynamic processes on carbonate chemistry.

720 The frequency of pH_T variability under ice cover was inconsistent. The PSD was weak overall
 721 during the closed phase but had a peak at 0.39 d^{-1} , which corresponded to a peak in temperature
 722 around the same frequency 0.36 d^{-1} . The temperature range of 1.9°C during the closed phase can
 723 affect carbonate chemistry thermodynamics potential modulating pH by ~ 0.036 ; however, this is
 724 less than the derived pH_T uncertainty. The other factor driving pH_T variability is biological
 725 respiration. Data sonde measurements of dissolved oxygen recorded in late April showed bottom
 726 waters reaching lows of $156.30 \mu\text{mol L}^{-1}$ (43 % saturation) compared to surface levels of 359.49
 727 $\mu\text{mol L}^{-1}$ (94 % saturation) (Table S1). The stratification of oxygen in this case can likely be
 728 associated with burgeoning PAR levels in April. Previous studies have shown increases in pH
 729 are associated with photosynthesis during ice-cover, which is more prevalent proximal to bulk
 730 ice resulting in higher pH at the surface compared to the bottom (Matson et al., 2014). Other
 731 factors driving pH variability could be due to the competition between anaerobic and aerobic
 732 metabolism in low oxygenated water, and the transfer of reduced metabolites from bioirrigation
 733 (Aller, 1982, 2001; Zakem et al., 2020). Efflux of reduced metabolites from the sediment can
 734 lead to high concentrations of reduced inorganic nitrogen if oxygen concentrations are low and
 735 oxidation processes slow (Aller, 2001; Middelburg and Levin, 2009). Discrete samples taken in
 736 April found high concentrations of reduced nitrogen in the bottom waters (Table S1). If oxygen
 737 levels begin to increase in late spring due to photosynthesis, the subsequent oxidation of nitrogen
 738 and other accumulated reduced metabolites could decrease pH as was seen from mid-April to
 739 mid-May. Due to limited under-ice sampling, however, there is no way to determine the
 740 trajectory of oxygen decrease or exact timing of under ice photosynthesis. The only other
 741 mechanism potentially supplying oxygen to the lagoon would be associated with water mass
 742 exchange via tide. According to the frequency analysis, there is limited evidence showing a

Deleted: 5.0

Deleted: mg

Deleted: 11.5

Deleted: mg

747 correlated frequency peak between pH_T and tide, indicating that tidal exchange may be restricted
748 or not a modulator of pH_T during the closed phase. Without measuring dissolved oxygen,
749 however, it remains unclear if oxygen is the determinant factor driving pH_T modification during
750 the closed phase.

751

752 4.6 Arctic lagoons as carbon source to atmosphere

753 The estimates of CO_2 flux during the open phases of 2018 and 2019 were an *a posteriori* method

754 to examine the drivers of pH variability in Kaktovik Lagoon. Following this approach,

755 comparisons between pH_T rate of change and estimated CO_2 flux did not correlate, suggesting

756 that outgassing rates were not significant enough to raise *in situ* pH. Rather, the analysis showed

757 that the estimated lagoon CO_2 flux varied substantially by year and appears at times to be a

758 source of CO_2 to the atmosphere. This is counter to other studies that measured carbon flux at a

759 lagoon in the far western Beaufort (Elson Lagoon), where this site was categorized as a carbon

760 sink; however, these lagoons differ in size, residence time, and connectivity to adjacent water

761 bodies (Lougheed et al., 2020). Overall, the western Arctic Ocean is thought to be a carbon sink (

762 [Laruelle et al., 2014](#); Evans et al., 2015a); although Mathis et al. (2012) described occasional

763 storm-induced upwelling events across the Beaufort Sea shelf that cause CO_2 efflux to the

764 atmosphere. In this study, the variability in estimated flux from the lagoon appeared to be a

765 function of baseline pH_T more than wind-driven stress. Open phase 2018 had a higher baseline

766 pH_T (8.01 – 8.18) than open phase 2019 (8.04 – 7.72), and despite wind speeds comparable to

767 open phase 2019, resulted in a lower estimated CO_2 efflux to the atmosphere. Conversely, open

768 phase 2019 maintained a lower baseline pH_T which promoted favorable disequilibrium (i.e.,

769 difference between $\text{PCO}_{2\text{sw}}$ and $\text{PCO}_{2\text{a}}$) conditions that only needed wind stress as a catalyst.

Formatted: Line spacing: Double

Deleted: ; Laruelle et al., 2014

Deleted:

Deleted: ess

773 Since flux preceded low pH_T values, and outgassing did not decrease hourly pH_T , the
 774 mechanisms driving low pH and PCO_2 —likely biological respiration— transcend the
 775 counterbalance of outgassing. Similar conclusions were found in a boreal lake where wind-
 776 driven stress reduced the thermocline and induced CO_2 upwelling that counterbalanced CO_2 loss
 777 from surface waters to the atmosphere (Åberg et al., 2010). In relation to this study, it would be
 778 logical to conclude that the reason wind speed was correlated to open phase 2019 and not open
 779 phase 2018 flux was due to a lower baseline pH and PCO_2 at the surface as a result of enhanced
 780 CO_2 upwelling from benthic respiration in the early portion of the open phase. Since open phase
 781 2018 measurements were taken in the latter portion of the season, benthic fluxes of CO_2 may
 782 have been exhausted as terrestrial OM abundance diminished with time.

783 _____ The flux estimates in this study suggest that the novel characteristics of coastal lagoons
 784 should be considered anomalous compared to the greater across shelf Arctic coast, defined as
 785 waters north of 70 °N and west of 100 °W (Bakker et al., 2014). The current classification of the
 786 coastal Arctic does not account for lagoons as specific ecosystems. Thus, the western Arctic
 787 coastal ocean is defined as a relatively homogenous area $1.2 \times 10^{12} \text{ m}^2$ along the Chukchi and
 788 Beaufort Seas extending 400 km offshore (Evans et al., 2015a). The coastal Beaufort Sea under
 789 this definition is estimated to have an annual mean carbon uptake of 8.5 Tg C yr^{-1} without ice,
 790 and a daily annual mean flux of $-2.1 \text{ mmol CO}_2 \text{ m}^{-2} \text{ d}^{-1}$ (Evans et al., 2015a). Recent evidence,
 791 however, has shown that previous estimates of the carbon sink capacity of the Arctic Ocean have
 792 been overestimated, suggesting that current and increasing riverine discharge will cause a
 793 reduction in A_T ultimately decreasing its potential to absorb CO_2 (Woosley and Millero, 2020).
 794 While the lagoon ecosystems comprise a small proportion of the greater Beaufort Sea shelf, they
 795 encompass > 50 % of its coastline with significant freshwater inputs that can lower the carbon

Commented [CM11]: Reviewer 1 B

Formatted: Subscript

Formatted: Subscript

Deleted: {Citation}

Formatted: Subscript

Formatted: Subscript

Formatted: Subscript

Deleted: ¶

Field Code Changed

798 sink capacity (Dunton et al., 2006; Woosley and Millero, 2020). It is suggested here that certain
 799 lagoons, including Kaktovik, are likely episodic sources of CO₂ to the atmosphere during open
 800 phases. The net daily average (\pm s.d.) CO₂ flux for Kaktovik Lagoon during open phase 2018 and
 801 2019 was -2.2 ± 6.5 and 14.6 ± 23.9 mmol CO₂ m⁻² d⁻¹, respectively. Over the entire calendar
 802 year that encompasses both open phases during which sensors were deployed, the annual daily
 803 average flux was 5.9 ± 19.3 mmol CO₂ m⁻² d⁻¹ for the entire calendar year. If integrated over the
 804 entire open phase (51.58 d in 2018 and 49.38 d in 2019), and the area of Kaktovik Lagoon,
 805 estimates suggest a net carbon flux of -2.68×10^{-5} Tg C open₁₈⁻¹ in open 2018 and 1.67×10^{-4} Tg
 806 C open₁₉⁻¹ in open 2019. Over an entire calendar year this equates to 1.40×10^{-4} Tg C yr⁻¹.
 807 It is noted that these estimates are for incomplete open phases as the data presented here do not
 808 comprise the entirety of each seasons due the scheduling of SeaFET deployment and recovery. If
 809 incorporating all the lagoons along the coast, it is plausible that the source of CO₂ from the
 810 lagoon ecosystems would partially offset the carbon sink capacity previously established,
 811 particularly when considering that the estimated daily annual average flux is at times
 812 substantially greater (5.9 ± 19.3 mmol CO₂ m⁻² d⁻¹), and opposite, of current estimates (-2.1
 813 mmol CO₂ m⁻² d⁻¹) (Evans et al., 2015a; Mathis et al., 2015). Further studies that can capture
 814 high-frequency carbonate chemistry variability are needed though to determine the degree and
 815 frequency of the Beaufort lagoon ecosystems' air-sea carbon exchange.

816 There is a fair amount of confidence in these estimates because the A_T-salinity correlation
 817 was robust ($R^2 = 0.968$) and the regression coefficients were proximal to other A_T-salinity
 818 regressions for the Gulf of Alaska and the western coastal Arctic, despite being derived from
 819 only three discrete samples (Yamamoto-Kawai et al., 2005; Shadwick et al., 2011; Evans et al.,
 820 2015b). Processes such as terrestrial runoff of organic alkalinity and ice-melt can increase

Commented [CM12]: Reviewer 1, C

Formatted: Font: 12 pt

Formatted: Font: 12 pt

Formatted: Indent: First line: 0"

Commented [CM13]: Reviewer 2 comment 1

Deleted: ; Shadwick et al., 2011; Yamamoto-Kawai et al., 2005...

823 uncertainties in the A_T -salinity relationship; however, ice-melt induced deviations appeared
 824 negligible in the Gulf of Alaska (Cai et al., 1998; Evans et al., 2014). Further, the overall
 825 uncertainty calculated as a flux potential was low. The main source of deviation was associated
 826 with higher PCO_2 values calculated from the A_T -salinity_{in situ} regression. This made up the upper
 827 bound of, thus, the conclusions drawn here are from the more conservative flux estimates. The
 828 effect of fresh water on the gas transfer velocity comprised the lower bound and was negligible
 829 overall. For the flux estimates presented here, a homogenous water column with respect to pH
 830 was assumed, given that discrete sonde measurements only showed pH stratification during the
 831 closed phase (Table S1). This is not to suggest that salinity and temperature driven stratification
 832 do not exist, rather that the evidence here suggests pH_T water column homogeneity. For example,
 833 pH_T during open phase 2018 did not correlate with salinity as values > 8.01 were present across a
 834 salinity range of 25. In cases where pH_T positively correlated with salinity as seen during open
 835 phase 2019, a freshwater stratification would suggest that low salinity at the surface would be
 836 associated with lower pH_T , and likely increase the CO_2 flux as there would be a greater
 837 disequilibrium between the lagoon and the air. According to the quadratic fit between pH_T and
 838 salinity, lower pH_T at the surface associated with freshwater stratification would outweigh the A_T
 839 estimates based on salinity by an order of magnitude if there was a salinity difference of 10
 840 between the surface and bottom waters. Thus, freshwater stratification at the surface would likely
 841 exceed our upper bound potential flux estimate and increase efflux rates. Further, any
 842 modulation of flux by temperature on the gas transfer velocity are less than the estimated upper
 843 bound and considered negligible.

Deleted: of the flux estimates

Deleted: uncertainty

Deleted: of the uncertainty

Deleted: ice-covered

Deleted: season

Deleted: uncertainty

Deleted: uncertainty

845 5 Conclusions

853 This study presents the first high-frequency pH time series for the open and under ice phases in
 854 the coastal Arctic lagoon system. Uncertainty estimates for pH_T were higher than desired but
 855 describe general trends and relative rates of change that are informative for understanding pH
 856 variability. The extremely low anomaly between the reference pH_T sample and the SeaFET
 857 suggest that the uncertainty is likely lower than estimated. pH can vary dramatically by year for
 858 the open phases and is likely a function of PAR availability and the amount of OM delivered
 859 from terrestrial sources as the balance between system autotrophy and heterotrophy were
 860 tenuous. This resulted in hourly pH_T rates of change > 0.4 units (~ 7.7 – 8.1). Under ice pH
 861 variability exhibited complexities, and we postulate that multiple drivers of pH variability such
 862 as carbonate chemistry thermodynamics, accumulation of respired CO₂, ikaite precipitation, and
 863 sediment efflux were all contributing mechanisms. It is apparent that further studies of carbonate
 864 chemistry dynamics at the sediment-water interface are needed to help elucidate porewater
 865 effects on bottom water pH variability during the closed, ice-covered phase, as well as
 866 continuous oxygen measurements. Estimated CO₂ outgassing during the open phase was not a
 867 significant factor driving pH_T variability due to the collinearity of wind stress and the infrequent
 868 convergence between disequilibrium and wind speed. However, carbon flux estimates suggest
 869 that the Beaufort lagoon ecosystems may be a substantial source of carbon to the atmosphere,
 870 which is counter to previous studies predicting coastal Arctic waters as a CO₂ sink. This may
 871 have further implications meaning that periods of CO₂ efflux from the lagoon system may
 872 increase as the extent of ice-free days increases in the coming decades with warmer temperatures.
 873 These results highlight the need for further investigation of the Beaufort lagoon ecosystems in
 874 the context of carbonate chemistry dynamics, as these processes can affect the diverse biological

Deleted: ice cover phase

Commented [CM14]: Reviewer 1, C

Formatted: Subscript

876 communities that are present here, and aid in understanding western coastal Arctic
877 biogeochemical dynamics. ▲

Formatted: Font color: Auto

878
879 **Data availability:** All data accessed from the Beaufort Lagoon Ecosystems LTER is available
880 on the Environmental Data initiative. See reference section for access links.

881

882 **Author Contributions:** Cale A. Miller, NM, CB, and ALK conceptualized the manuscript
883 thesis. CAM performed all data analysis and data visualization. ALK performed initial data

Deleted: the

884 QA/QC for pH data. ALK, NM, and CB performed lab analyses. CAM wrote the original
885 manuscript draft with minor contributions in the introduction from ALK and CB in the methods.

Deleted: Cale A. Miller performed all data analysis.

886 ALK, CB, and NM reviewed and edited the manuscript.

887

888 **Competing interests:** The authors declare no conflict of interest.

889

890 **Acknowledgments:** We thank R/V Proteus captains Ted Dunton and John Dunton for expert
891 mooring deployment and recovery. We additionally thank K. Dunton, S. Jump, J. Kasper for
892 logistical and field assistance. This work took place in the traditional and current homeland of
893 the Kaktovikmuit.

894

897 **Financial support:** This material is based upon work supported by the National Science
898 Foundation under award #1656026

899
900 **References**

- 901 Åberg, J., Jansson, M. and Jonsson, A.: Importance of water temperature and thermal
902 stratification dynamics for temporal variation of surface water CO₂ in a boreal lake, J. Geophys.
903 Res. Biogeosciences, 115(G2), doi:https://doi.org/10.1029/2009JG001085, 2010.
- 904 Aller, R.: Carbonate Dissolution in Nearshore Terrigenous Muds - the Role of Physical and
905 Biological Reworking, J. Geol., 90(1), 79–95, 1982.
- 906 Aller, R.C.: Transport and reactions in the bioirrigated zone, in: The Benthic Boundary Layer:
907 Transport Processes and Biogeochemistry, edited by: Boudreau, B. P. and Jorgensen, B. B., pp.
908 269–301, Oxford University Press., 2001.
- 909 Bakker, D. C. E., Pfeil, B., Smith, K., Hankin, S., Olsen, A., Alin, S. R., Cosca, C., Harasawa, S.,
910 Kozyr, A., Nojiri, Y., O'Brien, K. M., Schuster, U., Telszewski, M., Tilbrook, B., Wada, C., Akl,
911 J., Barbero, L., Bates, N. R., Boutin, J., Bozec, Y., Cai, W.-J., Castle, R. D., Chavez, F. P., Chen,
912 L., Chierici, M., Currie, K., de Baar, H. J. W., Evans, W., Feely, R. A., Fransson, A., Gao, Z.,
913 Hales, B., Hardman-Mountford, N. J., Hoppema, M., Huang, W.-J., Hunt, C. W., Huss, B.,
914 Ichikawa, T., Johannessen, T., Jones, E. M., Jones, S. D., Jutterström, S., Kitidis, V., Körtzinger,
915 A., Landschützer, P., Lauvset, S. K., Lefèvre, N., Manke, A. B., Mathis, J. T., Merlivat, L.,
916 Metzl, N., Murata, A., Newberger, T., Omar, A. M., Ono, T., Park, G.-H., Paterson, K., Pierrot,
917 D., Ríos, A. F., Sabine, C. L., Saito, S., Salisbury, J., Sarma, V. V. S. S., Schlitzer, R., Sieger, R.,
918 Skjelvan, I., Steinhoff, T., Sullivan, K. F., Sun, H., Sutton, A. J., Suzuki, T., Sweeney, C.,
919 Takahashi, T., Tjiputra, J., Tsurushima, N., van Heuven, S. M. a. C., Vandemark, D., Vlahos, P.,
920 Wallace, D. W. R., Wanninkhof, R. and Watson, A. J.: An update to the Surface Ocean CO₂
921 Atlas (SOCAT version 2), Earth Syst. Sci. Data, 6(1), 69–90, doi:https://doi.org/10.5194/essd-6-
922 69-2014, 2014.
- 923 Beaufort Lagoon Ecosystems LTER and J. Kasper. 2020. Circulation dynamics: currents, waves,
924 temperature measurements from moorings in lagoon sites along the Alaska Beaufort Sea coast,
925 2018-ongoing ver 2. Environmental Data Initiative.
926 https://doi.org/10.6073/pasta/3475cdabb160a9f844aa5ede627c5f6fc
927
- 928 Beaufort Lagoon Ecosystems LTER, Core Program. 2020. Photosynthetically active radiation
929 (PAR) time series from lagoon sites along the Alaska Beaufort Sea coast, 2018-ongoing ver 1.
930 Environmental Data Initiative.
931 https://doi.org/10.6073/pasta/cedd430d430d9149b9d7f1919729
932
- 933 Beaufort Lagoon Ecosystems LTER, Core Program. 2020. physicochemical water column
934 parameters and hydrographic time series from river, lagoon, and open ocean sites along the

Formatted: Subscript

Alaska Beaufort Sea coast, 2018-ongoing ver 1. Environmental Data Initiative.
<https://doi.org/10.6073/pasta/e0e71c2d59bf7b08928061f546be6a9a>

Beaufort Lagoon Ecosystems LTER, Core Program. 2020. Time series of water column pH from lagoon sites along the Alaska Beaufort Sea coast, 2018-ongoing ver 1. Environmental Data Initiative. <https://doi.org/10.6073/pasta/9305328d0f1ed28fbb2d7cf56c686786>

Bresnahan, P. J., Martz, T. R., Takeshita, Y., Johnson, K. S. and LaShomb, M.: Best practices for autonomous measurement of seawater pH with the Honeywell Durafet, *Methods Oceanogr.*, 9, 44–60, doi:10.1016/j.mio.2014.08.003, 2014.

Cai, W.-J., Wang, Y. and Hodson, R. E.: Acid-Base Properties of Dissolved Organic Matter in the Estuarine Waters of Georgia, USA, *Geochim. et Cosmochim. Acta*, 62(3), 473–483, doi:10.1016/S0016-7037(97)00363-3, 1998.

Cai, W.-J. and Wang, Y.: The chemistry, fluxes, and sources of carbon dioxide in the estuarine waters of the Satilla and Altamaha Rivers, Georgia, *Limnology and Oceanography*, 43(4), 657–668, doi:<https://doi.org/10.4319/lo.1998.43.4.0657>, 1998.

Cai, W.-J.: Estuarine and Coastal Ocean Carbon Paradox: CO₂ Sinks or Sites of Terrestrial Carbon Incineration?, in *Annual Review of Marine Science*, Vol 3, vol. 3, edited by C. A. Carlson and S. J. Giovannoni, pp. 123–145, Annual Reviews, Palo Alto., 2011.

Capuzzo, E., Stephens, D., Silva, T., Barry, J. and Forster, R. M.: Decrease in water clarity of the southern and central North Sea during the 20th century, *Glob. Change Biol.*, 21(6), 2206–2214, doi:10.1111/gcb.12854, 2015.

Carstensen, J. and Duarte, C. M.: Drivers of pH Variability in Coastal Ecosystems, *Environ. Sci. Technol.*, 53(8), 4020–4029, doi:10.1021/acs.est.8b03655, 2019.

Craig, P. C.: Subsistence fisheries at coastal villages in the Alaskan Arctic, 1970–1986. *Biological Papers of the University of Alaska*, 24, 131–152, 1989.

Cyronak, T., Takeshita, Y., Courtney, T. A., DeCarlo, E. H., Eyre, B. D., Kline, D. I., Martz, T., Page, H., Price, N. N., Smith, J., Stoltenberg, L., Tresguerres, M. and Andersson, A. J.: Diel temperature and pH variability scale with depth across diverse coral reef habitats, *Limnol. Oceanogr. Lett.*, 5(2), 193–203, doi:10.1002/lol2.10129, 2020.

Dickson, A.: Thermodynamics of the Dissociation of Boric-Acid in Potassium-Chloride Solutions from 273.15-K to 318.15-K, *J. Chem. Eng. Data*, 35(3), 253–257, doi:10.1021/je00061a009, 1990.

Dickson A. G., Sabine C. L. & Christian J. R.: Guide to best practices for ocean CO₂ measurements, in: *PICES Special Publication*, edited by: Dickson, A. G., Sabine, C. L., and Christian, J. R., 2007.

Formatted: Font: (Default) Times New Roman

Formatted: Font: (Default) Times New Roman

Formatted: Font: (Default) Times New Roman

Formatted: Normal

Formatted: Font: (Default) Times New Roman

Formatted: Subscript

- Dinauer, A. and Mucci, A.: Spatial variability in surface-water $p\text{CO}_2$ and gas exchange in the world's largest semi-enclosed estuarine system: St. Lawrence Estuary (Canada), *Biogeosciences*, 14(13), 3221–3237, doi:https://doi.org/10.5194/bg-14-3221-2017, 2017.
- Douglas, N. K. and Byrne, R. H.: Achieving accurate spectrophotometric pH measurements using unpurified meta-cresol purple, *Mar. Chem.*, 190, 66–72, doi:10.1016/j.marchem.2017.02.004, 2017.
- Dunton, K.H., and S.V. Schonberg.: Barter Island to Demarcation Bay: A preliminary benthic survey of Arctic coastal lagoons. Fairbanks: Final Report to USF&WS, Arctic Refuge, 2006.
- Dunton, K. H., Weingartner, T. and Carmack, E. C.: The nearshore western Beaufort Sea ecosystem: Circulation and importance of terrestrial carbon in arctic coastal food webs, *Prog. Oceanogr.*, 71(2), 362–378, doi:10.1016/j.pocean.2006.09.011, 2006.
- Dunton, K. H., Schonberg, S. V. and Cooper, L. W.: Food Web Structure of the Alaskan Nearshore Shelf and Estuarine Lagoons of the Beaufort Sea, *Estuaries Coasts*, 35(2), 416–435, doi:10.1007/s12237-012-9475-1, 2012.
- Evans, W., Mathis, J. T. and Cross, J. N.: Calcium carbonate corrosivity in an Alaskan inland sea, *Biogeosciences*, 11(2), 365–379, doi:10.5194/bg-11-365-2014, 2014.
- Evans, W., Mathis, J. T., Cross, J. N., Bates, N. R., Frey, K. E., Else, B. G. T., Papkyriakou, T. N., DeGrandpre, M. D., Islam, F., Cai, W.-J., Chen, B., Yamamoto-Kawai, M., Carmack, E., Williams, W. J. and Takahashi, T.: Sea-air CO_2 exchange in the western Arctic coastal ocean, *Glob. Biogeochem. Cy.*, 29(8), 1190–1209, doi:10.1002/2015GB005153, 2015a.
- Evans W., Mathis, J. T., Ramsey, J. and Hetrick J.: On the frontline: Tracking ocean acidification in an Alaskan shellfish hatchery, *PloS One*, 10(7), e0130384, doi:10.1371/journal.pone.0130384, 2015b.
- Fabry, V., McClintock, J., Mathis, J. and Grebmeier, J.: Ocean Acidification at High Latitudes: The Bellwether, *Oceanogr.*, 22(4), 160–171, doi:10.5670/oceanog.2009.105, 2009.
- Fransson, A., Chierici, M., Miller, L. A., Carnat, G., Shadwick, E., Thomas, H., Pineault, S. and Papakyriakou, T. N.: Impact of sea-ice processes on the carbonate system and ocean acidification at the ice-water interface of the Amundsen Gulf, Arctic Ocean, *J. Geophys. Res. Oceans*, 118(12), 7001–7023, doi:10.1002/2013JC009164, 2013.
- Gonski, S. F., Cai, W.-J., Ullman, W. J., Joesoef, A., Main, C. R., Pettay, D. T. and Martz, T. R.: Assessment of the suitability of DuraFet-based sensors for pH measurement in dynamic estuarine environments, *Estuar. Coast. Shelf Sci.*, 200, 152–168, doi:10.1016/j.ecss.2017.10.020, 2018.
- Griffiths, W.B., J.K. Den Beste, and P.C.: Fisheries investigations in a coastal lagoon region of the Beaufort Sea (Kaktovik Lagoon, Alaska). *Arctic Gas Biol. Report Ser.* 40(2): 1–190, 1977.

1013 [Hagens, M., Hunter, K. A., Liss, P. S. and Middelburg, J. J.: Biogeochemical context impacts](#)
 1014 [seawater pH changes resulting from atmospheric sulfur and nitrogen deposition, *Geophys. Res.*](#)
 1015 [Lett., 41\(3\), 935–941, doi:10.1002/2013GL058796, 2014.](#)

1016 [Hales, B., Suhrbier, A., Waldbusser, G. G., Feely, R. A. and Newton, J. A.: The Carbonate](#)
 1017 [Chemistry of the “Fattening Line,” Willapa Bay, 2011–2014, *Estuar. Coast.*, 1–14,](#)
 1018 [doi:10.1007/s12237-016-0136-7, 2016.](#)

1019 [Hare, A. A., Wang, F., Barber, D., Geilfus, N.-X., Galley, R. J. and Rysgaard, S.: pH evolution](#)
 1020 [in sea ice grown at an outdoor experimental facility, *Mar. Chem.*, 154, 46–54,](#)
 1021 [doi:10.1016/j.marchem.2013.04.007, 2013.](#)

1022 [Harris, C. M., McClelland, J. W., Connelly, T. L., Crump, B. C. and Dunton, K. H.: Salinity and](#)
 1023 [Temperature Regimes in Eastern Alaskan Beaufort Sea Lagoons in Relation to Source Water](#)
 1024 [Contributions, *Estuar. Coast.*, 40\(1\), 50–62, doi:10.1007/s12237-016-0123-z, 2017.](#)

1025 [Harris, C. M., McTigue, N. D., McClelland, J. W. and Dunton, K. H.: Do high Arctic coastal](#)
 1026 [food webs rely on a terrestrial carbon subsidy?, *Food Webs*, 15, e00081,](#)
 1027 [doi:10.1016/j.fooweb.2018.e00081, 2018.](#)

1028 [Hofmann, G. E., Smith, J. E., Johnson, K. S., Send, U., Levin, L. A., Micheli, F., Paytan, A.,](#)
 1029 [Price, N. N., Peterson, B., Takeshita, Y., Matson, P. G., Crook, E. D., Kroeker, K. J., Gambi, M.](#)
 1030 [C., Rivest, E. B., Frieder, C. A., Yu, P. C. and Martz, T. R.: High-Frequency Dynamics of Ocean](#)
 1031 [pH: A Multi-Ecosystem Comparison, *Plos One*, 6\(12\), e28983,](#)
 1032 [doi:10.1371/journal.pone.0028983, 2011.](#)

1033 [Johnson, S. W., Thedinga, J. F., Neff, A. D., & Hoffman, C. A.: Fish fauna in nearshore waters](#)
 1034 [of a barrier island in the western Beaufort Sea, Alaska, 2010.](#)

1035
 1036 [Kapsenberg, L. and Hofmann, G. E.: Ocean pH time-series and drivers of variability along the](#)
 1037 [northern Channel Islands, California, USA, *Limnol. Oceanogr.*, 61\(3\), 953–968,](#)
 1038 [doi:10.2307/26628461, 2016.](#)

1039
 1040 [Kapsenberg, L., Kelley, A. L., Shaw, E. C., Martz, T. R. and Hofmann, G. E.: Near-shore](#)
 1041 [Antarctic pH variability has implications for the design of ocean acidification experiments, *Sci.*](#)
 1042 [Rep., 5, srep09638, doi:10.1038/srep09638, 2015.](#)

1043
 1044 [Kinney, P., Schell, D., Dygas, J., Nenahlo, R. and Hall, G.: Nearshore Currents, in: Baseline data](#)
 1045 [study of the Alaskan Arctic aquatic environment, Kinney, P., Schell, D., Alexander, V., Burrell,](#)
 1046 [D., Cooney, R. and Naidu, A. S., Univ. Alaska, Inst. Mar. Sci. Rep. R-72-3, 1971.](#)

1047
 1048 [Kraus, N. C., Patsch, K. and Munger, S.: Barrier Beach Breaching from the Lagoon Side, With](#)
 1049 [Reference to Northern California, U.S. Army Engineer Research and Development Center, Coast](#)
 1050 [and Hydraulics Laboratory, 2008.](#)

1051

1052 [Laruelle, G. G., Lauerwald, R., Pfeil, B. and Regnier, P.: Regionalized global budget of the CO₂](#)
 1053 [exchange at the air-water interface in continental shelf seas, *Glob. Biogeochem. Cy.*, 28\(11\),](#)
 1054 [1199–1214, doi:10.1002/2014GB004832, 2014.](#)

1055 [Lissauer, I. M., Hachmeister, L. E., Morson, B. J.: Atlas of the Beaufort Sea, U.S. Dep. of Trans.,](#)
 1056 [U.S. Coast Guard, Office of Res. and Dev., 1984.](#)

1057 [Lougheed, V. L., Tweedie, C. E., Andresen, C. G., Armendariz, A.M., Escarzaga, S. M. and](#)
 1058 [Tarin, G.: Patterns and drivers of carbon dioxide concentration sin aquatic ecosystems of the](#)
 1059 [Arctic coastal tundra, *Glob. Biogeochem. Cy.*, 34\(3\), e2020GB006552,](#)
 1060 [doi:10.1029/2020GB006552, 2020.](#)

1061 [Lueker, T. J., Dickson, A. G. and Keeling, C. D.: Ocean pCO₂ calculated from dissolved](#)
 1062 [inorganic carbon, alkalinity, and equations for K₁ and K₂: Validation based on laboratory](#)
 1063 [measurements of CO₂ in gas and seawater at equilibrium, *Mar. Chem.*, 70\(1\), 105–119,](#)
 1064 [doi:10.1016/S0304-4203\(00\)00022-0, 2000.](#)

1065 [Macdonald, R.W., E. Sakshaug, and R. Stein.: The Arctic Ocean: modern status and recent](#)
 1066 [climate change, in: The organic carbon cycle in the Arctic Ocean, edited by: R. Stein and R.W.](#)
 1067 [Macdonald, pp. 6–21, Berlin: Springer, 2004.](#)

1068 [Martz, T. R., Connery, J. G. and Johnson, K. S.: Testing the Honeywell Durafet® for seawater](#)
 1069 [pH applications, *Limnol. Oceanogr. Methods*, 8\(5\), 172–184, doi:10.4319/lom.2010.8.172, 2010.](#)

1070 [Mathis, J. T., Pickart, R. S., Byrne, R. H., McNeil, C. L., Moore, G. W. K., Juranek, L. W., Liu,](#)
 1071 [X., Ma, J., Easley, R. A., Elliot, M. M., Cross, J. N., Reisdorph, S. C., Bahr, F., Morison, J.,](#)
 1072 [Lichendorf, T. and Feely, R. A.: Storm-induced upwelling of high pCO₂ waters onto the](#)
 1073 [continental shelf of the western Arctic Ocean and implications for carbonate mineral saturation](#)
 1074 [states, *Geophys. Res. Lett.*, 39\(7\), L07606, doi:10.1029/2012GL051574, 2012.](#)

1075 [Mathis, J. T., Cross, J. N., Evans, W. and Doney, S. C.: Ocean Acidification in the Surface](#)
 1076 [Waters of the Pacific-Arctic Boundary Regions, *Oceanogr.*, 28\(2\), 122–135,](#)
 1077 [doi:10.5670/oceanog.2015.36, 2015.](#)

1078 [Matson, P. G., Washburn, L., Martz, T. R. and Hofmann, G. E.: Abiotic versus Biotic Drivers of](#)
 1079 [Ocean pH Variation under Fast Sea Ice in McMurdo Sound, Antarctica, *PloS One*, 9\(9\),](#)
 1080 [e107239, doi:10.1371/journal.pone.0107239, 2014.](#)

1081 [Matthews, J. B. and Stringer, W. J.: Spring breakup and flushing of an Arctic lagoon estuary, *J.*](#)
 1082 [Geophys. Res. Oceans, 89\(C2\), 2073–2079, doi:10.1029/JC089iC02p02073, 1984.](#)

1083 [McClelland, J. W., Déry, S. J., Peterson, B. J., Holmes, R. M. and Wood, E. F.: A pan-arctic](#)
 1084 [evaluation of changes in river discharge during the latter half of the 20th century, *Geophys. Res.*](#)
 1085 [Lett., 33\(6\), doi:10.1029/2006GL025753, 2006.](#)

1086 [McClelland, J. W., Holmes, R. M., Dunton, K. H. and Macdonald, R. W.: The Arctic Ocean](#)
 1087 [Estuary, *Estuar. Coast.*, 35\(2\), 353–368, doi:10.1007/s12237-010-9357-3, 2012.](#)

1088
 1089
 1090

1091 [McClelland, J. W., Townsend-Small, A., Holmes, R. M., Pan, F., Stieglitz, M., Khosh, M. and](#)
1092 [Peterson, B. J.: River export of nutrients and organic matter from the North Slope of Alaska to](#)
1093 [the Beaufort Sea, *Water Resour. Res.*, 50\(2\), 1823–1839, doi:10.1002/2013WR014722, 2014.](#)
1094
1095 [McLaughlin, K., Dickson, A., Weisberg, S. B., Coale, K., Elrod, V., Hunter, C., Johnson, K. S.,](#)
1096 [Kram, S., Kudela, R., Martz, T., Negrey, K., Passow, U., Shaughnessy, F., Smith, J. E., Tadesse,](#)
1097 [D., Washburn, L. and Weis, K. R.: An evaluation of ISFET sensors for coastal pH monitoring](#)
1098 [applications, *Reg. Stud. Mar. Sci.*, 12, 11–18, doi:10.1016/j.rsma.2017.02.008, 2017.](#)
1099
1100 [Middelburg, J. J. and Levin, L. A.: Coastal hypoxia and sediment biogeochemistry,](#)
1101 [Biogeosciences, 6\(7\), 1273–1293, doi:https://doi.org/10.5194/bg-6-1273-2009, 2009.](#)
1102
1103 [Miller, C. A., Pocock, K., Evans, W. and Kelley, A. L.: An evaluation of the performance of](#)
1104 [Sea-Bird Scientific’s SeaFET™ autonomous pH sensor: considerations for the broader](#)
1105 [oceanographic community, *Ocean Sci.*, 14\(4\), 751–768, doi:https://doi.org/10.5194/os-14-751-](#)
1106 [2018, 2018.](#)
1107
1108 [Miller, C. A. and Kelley A. K.: Seasonality and biological forcing the diel frequency of](#)
1109 [nearshore pH extremes in a sub-arctic Alaskan estuary, *Limnol. Oceanogr.*, *in press*, doi:](#)
1110 [10.1002/lno.11698, 2021.](#)
1111
1112 [Miller, L. A., Carnat, G., Else, B. G. T., Sutherland, N. and Papakyriakou, T. N.: Carbonate](#)
1113 [system evolution at the Arctic Ocean surface during autumn freeze-up, *J. Geophys. Res. Oceans*,](#)
1114 [116\(C9\), doi:10.1029/2011JC007143, 2011.](#)
1115
1116 [Miller, L. A., Macdonald, R. W., McLaughlin, F., Mucci, A., Yamamoto-Kawai, M., Giesbrecht,](#)
1117 [K. E. and Williams, W. J.: Changes in the marine carbonate system of the western Arctic:](#)
1118 [patterns in a rescued data set, *Polar Res.*, 33\(1\), 20577, doi:10.3402/polar.v33.20577, 2014.](#)
1119
1120 [Mincks, S. L., Smith, C. R. and DeMaster, D. J.: Persistence of labile organic matter and](#)
1121 [microbial biomass in Antarctic shelf sediments: evidence of a sediment ‘food bank,’ *Marine*](#)
1122 [Ecol. Prog. Ser., 300, 3–19, 2005.](#)
1123
1124 [Moriarty, J. M., Harris, C. K., Friedrichs, M. A. M., Fennel, K. and Xu, K.: Impact of Seabed](#)
1125 [Resuspension on Oxygen and Nitrogen Dynamics in the Northern Gulf of Mexico: A Numerical](#)
1126 [Modeling Study, *J. Geophys. Res. Oceans*, 123\(10\), 7237–7263, doi:10.1029/2018JC013950,](#)
1127 [2018.](#)
1128
1129 [Mouillot, D., Dumay, O. and Tomasini, J. A.: Limiting similarity, niche filtering and functional](#)
1130 [diversity in coastal lagoon fish communities, *Estuar. Coast. Shelf Sci.*, 71\(3\), 443–456,](#)
1131 [doi:10.1016/j.ecss.2006.08.022, 2007.](#)
1132
1133 [Muth, A., Kelley, A. K. and Dunton, K.: High-Frequency pH Time-Series Reveals Pronounced](#)
1134 [Seasonality in Arctic Coastal Waters, *Limnol. Oceanogr.*, *in review*.](#)

Formatted: Normal

Formatted: Normal

1129 [Nomura, D., Yoshikawa-Inoue, H. and Toyota, T.: The effect of sea-ice growth on air-sea CO₂](#)
 1130 [flux in a tank experiment, Tellus B Chem. Phys. Meteorol., 58\(5\), 418–426, doi:10.1111/j.1600-](#)
 1131 [0889.2006.00204.x, 2006.](#)

1132 [Orr, J. C., Epitalon, J.-M., Dickson, A. G. and Gattuso, J.-P.: Routine uncertainty propagation for](#)
 1133 [the marine carbon dioxide system, Mar. Chem., 207, 84–107,](#)
 1134 [doi:10.1016/j.marchem.2018.10.006, 2018.](#)

1135 [Papadimitriou, S., Kennedy, H., Kattner, G., Dieckmann, G. S. and Thomas, D. N.: Experimental](#)
 1136 [evidence for carbonate precipitation and CO₂ degassing during sea ice formation, Geochim.](#)
 1137 [Cosmochim. Acta, 68\(8\), 1749–1761, doi:10.1016/j.gca.2003.07.004, 2004.](#)

1138 [Qi, D., Chen, L., Chen, B., Gao, Z., Zhong, W., Feely, R. A., Anderson, L. G., Sun, H., Chen, J.,](#)
 1139 [Chen, M., Zhan, L., Zhang, Y. and Cai, W.-J.: Increase in acidifying water in the western Arctic](#)
 1140 [Ocean, Nat. Clim. Change, 7\(3\), 195–199, doi:10.1038/nclimate3228, 2017.](#)

1141 [Rassmann, J., Eitel, E. M., Lansard, B., Cathalot, C., Brandily, C., Taillefert, M. and Rabouille,](#)
 1142 [C.: Benthic alkalinity and dissolved inorganic carbon fluxes in the Rhône River prodelta](#)
 1143 [generated by decoupled aerobic and anaerobic processes, Biogeosciences, 17\(1\), 13–33,](#)
 1144 [doi:https://doi.org/10.5194/bg-17-13-2020, 2020.](#)

1145 [Rivest, E. B., O'Brien, M., Kapsenberg, L., Gotschalk, C. C., Blanchette, C. A., Hoshijima, U.](#)
 1146 [and Hofmann, G. E.: Beyond the benchtop and the benthos: Dataset management planning and](#)
 1147 [design for time series of ocean carbonate chemistry associated with Durafet®-based pH sensors,](#)
 1148 [Ecol. Inform., Complete\(36\), 209–220, doi:10.1016/j.ecoinf.2016.08.005, 2016.](#)

1149 [Robards, M. D.: Coastal lagoon community and ecological monitoring in the Southern](#)
 1150 [Chukchi Sea National Park Unit over five decades- Status and 2012 field sampling report.](#)
 1151 [National Park Service, Fairbanks, AK, 2014.](#)

1152

1153 [Rysgaard, S., Glud, R. N., Lennert, K., Cooper, M., Halden, N., Leakey, R. J. G., Hawthorne,](#)
 1154 [F.C. and Barber, D.: Ikaite crystals in melting sea ice - implications for pCO₂ and pH levels in](#)
 1155 [Arctic surface waters, The Cryos., 6, 901–908, doi:10.5194/tc-6-901-2012, 2012.](#)

1156 [Salisbury, J. E., Vandemark, D., Hunt, C. W., Campbell, J. W., McGillis, W. R. and McDowell,](#)
 1157 [W. H.: Seasonal observations of surface waters in two Gulf of Maine estuary-plume systems:](#)
 1158 [Relationships between watershed attributes, optical measurements and surface pCO₂, Estuar.](#)
 1159 [Coast. Shelf Sci., 77\(2\), 245–252, doi:10.1016/j.ecss.2007.09.033, 2008.](#)

1160 [Schreiner, K. M., Bianchi, T. S., Eglinton, T. I., Allison, M. A. and Hanna, A. J. M.: Sources of](#)
 1161 [terrigenous inputs to surface sediments of the Colville River Delta and Simpson's Lagoon,](#)
 1162 [Beaufort Sea, Alaska, J. Geophys. Res. Biogeosciences, 118\(2\), 808–824,](#)
 1163 [doi:10.1002/jgrg.20065, 2013.](#)

1164 [Shadwick, E. H., Thomas, H., Chierici, M., Else, B., Fransson, A., Michael, C., Miller, L. A.,](#)
 1165 [Mucci, A., Niemi, A., Papakyriakou, T. N. and Tremblay, J.-E.: Seasonal variability of the](#)
 1166 [inorganic carbon system in the Amundsen Gulf region of the southeastern Beaufort Sea, Limnol.](#)
 1167 [Oceanogr., 56\(1\), 303–322, doi:10.4319/lo.2011.56.1.0303, 2011.](#)

1168
 1169 Stein, R. and Macdonald, R. W.: Organic carbon budget: Arctic Ocean vs. Global Ocean
 1170 in: The organic carbon cycle in the Arctic Ocean, edited by: R. Stein and R.W. Macdonald, pp.
 1171 315–322, Berlin: Springer, 2004.

1172 Sulpis, O., Lauvset, S. K. and Hagens, M.: Current estimates of K_1^* and K_2^* appear inconsistent
 1173 with measured CO_2 system parameters in cold oceanic regions, Ocean Science, 16(4), 847–862,
 1174 doi:https://doi.org/10.5194/os-16-847-2020, 2020.

1175 Takeshita, Y., Frieder, C. A., Martz, T. R., Ballard, J. R., Feely, R. A., Kram, S., Nam, S.,
 1176 Navarro, M. O., Price, N. N. and Smith, J. E.: Including high-frequency variability in coastal
 1177 ocean acidification projections, Biogeosciences, 12(19), 5853–5870,
 1178 doi:https://doi.org/10.5194/bg-12-5853-2015, 2015.

1180 Thoning, K. W., Crotwell, A. M. and J. W. Mund.: Atmospheric Carbon Dioxide Dry Air Mole
 1181 Fractions from continuous measurements at Mauna Loa, Hawaii, Barrow, Alaska, American
 1182 Samoa, and South Pole. 1973-2019, Version 2020-08 Notional Oceanic and Atmospheric
 1183 Administration (NOAA), Global Monitoring Laboratory (GML), Boulder, Colorado, USA
 1184 http://doi.org/10.151138/yaf1-bk21 FTP pat:
 1185 ftp://aftp.cmdl.noaa.gov/data/greenhouse_gases/co2/in-situ/surface/

1186
 1187 Tibbles, M.: The seasonal dynamics of coastal Arctic lagoons in Northwest Alaska, M.Sc. thesis,
 1188 December. College of Fisheries and Ocean Sciences, University of Alaska Fairbanks, 2018.

1189 Uppström, L. R.: The boron/chlorinity ratio of deep-sea water from the Pacific Ocean, Deep Sea
 1190 Res. Oceanogr. Abstr., 21, 161–162, doi:10.1016/0011-7471(74)90074-6, 1974.

1191 van Heuven, S., Pierrot, D., Rae, J. W. B., Lewis, E., and Wallace,
 1192 D.W. R.: MATLAB Program Developed for CO_2 System Calculations Department of Energy,
 1193 Oak Ridge, Tennessee, 2011.

1194
 1195 Wanninkhof, R.: Relationship between wind speed and gas exchange over the ocean revisited,
 1196 Limnol. Oceanogr. Methods, 12(6), 351–362, doi:10.4319/lom.2014.12.351, 2014.

1197 Woosley, R. J. and Millero, F. J.: Freshening of the western Arctic negates anthropogenic carbon
 1198 uptake potential, Limnol. Oceanogr., 65(8), 1834–1846, doi:10.1002/lno.11421, 2020.

1199 Wynn, J. G., Robbins, L. L. and Anderson, L. G.: Processes of multibathyal aragonite
 1200 undersaturation in the Arctic Ocean, J. Geophys. Res. Oceans, 121(11), 8248–8267,
 1201 doi:10.1002/2016JC011696, 2016.

1202 Yamamoto-Kawai, M., Tanaka, N. and Pivovarov, S.: Freshwater and brine behaviors in the
 1203 Arctic Ocean deduced from historical data of δO^{18} and alkalinity (1922–2022 A.D.), J. Geophys.
 1204 Res. Oceans, 110(C10), doi:10.1029/2004JC002793, 2005.

1205

Formatted: Font: (Default) Times New Roman

Formatted: Font color: Auto

Formatted: Normal

1206 [Zakem, E. J., Mahadevan, A., Lauderdale, J. M. and Follows, M. J.: Stable aerobic and anaerobic](#)
1207 [coexistence in anoxic marine zones, ISME J., 14\(1\), 288–301, doi:10.1038/s41396-019-0523-8,](#)
1208 [2020.](#)

1209 [Zeebe, R. E. and Wolf-Gladrow, D. A.: CO₂ in seawater equilibrium, kinetics, isotopes, Elsevier,](#)
1210 [Amsterdam; New York., 2001.](#)

1211 [Zhang, Y., Yamamoto-Kawai, M. and Williams, W. J.: Two Decades of Ocean Acidification in](#)
1212 [the Surface Waters of the Beaufort Gyre, Arctic Ocean: Effects of Sea Ice Melt and Retreat From](#)
1213 [1997–2016, Geophys. Res. Lett., 47\(3\), e60119, doi:10.1029/2019GL086421, 2020.](#)
1214
1215
1216

1217 **Table 1.** Calibration and reference bottle data for SeaFET. Propagated uncertainty, for each
1218 bottle, and the calculated total pH uncertainty value as overall average (in bold). **Value marked**
1219 **with * indicates the calibration bottle sample.**

<i>Date & Time</i>	<i>Source</i>	<i>pH_T</i> <i>internal electrode</i>	<i>Propagated</i> <i>uncertainty</i>	<i>Anomaly:</i> <i> bottle sample - SeaFET </i>
17 Aug. 2018	SeaFET	8.076	—	—
	Bottle sample	8.073*	0.1600	
26 Apr. 2018	SeaFET	7.576	—	0.0061
	Bottle sample	7.582	0.1006	
Total uncertainty				0.0889

1220
1221
1222
1223
1224
1225
1226
1227

Deleted: Aller, R.: Carbonate Dissolution in Nearshore Terrigenous Muds - the Role of Physical and Biological Reworking, J. Geol., 90(1), 79–95, 1982. [¶](#)

Aller, R.C.: Transport and reactions in the bioirrigated zone, in: The Benthic Boundary Layer: Transport Processes and Biogeochemistry, edited by: Boudreau, B. P. and Jorgensen, B. B., pp. 269–301, Oxford University Press., 2001. [¶](#)

Bakker, D. C. E., Pfeil, B., Smith, K., Hankin, S., Olsen, A., Alin, S. R., Cosca, C., Harasawa, S., Kozyr, A., Nojiri, Y., O'Brien, K. M., Schuster, U., Telszewski, M., Tilbrook, B., Wada, C., Akl, J., Barbero, L., Bates, N. R., Boutin, J., Bozec, Y., Cai, W.-J., Castle, R. D., Chavez, F. P., Chen, L., Chierici, M., Currie, K., de Baar, H. J. W., Evans, W., Feely, R. A., Fransson, A., Gao, Z., Hales, B., Hardman-Mountford, N. J., Hoppema, M., Huang, W.-J., Hunt, C. W., Huss, B., Ichikawa, T., Johannessen, T., Jones, E. M., Jones, S. D., Jutterström, S., Kitidis, V., Körtzinger, A., Landschützer, P., Lauvset, S. K., Lefèvre, N., Manke, A. B., Mathis, J. T., Merlivat, L., Metzl, N., Murata, A., Newberger, T., Omar, A. M., Ono, T., Park, G.-H., Paterson, K., Pierrot, D., Rios, A. F., Sabine, C. L., Saito, S., Salisbury, J., Sarma, V. V. S. S., Schlitzer, R., Sieger, R., Skjelvan, I., Steinhoff, T., Sullivan, K. F., Sun, H., Sutton, A. J., Suzuki, T., Sweeney, C., Takahashi, T., Tjiputra, J., Tsurushima, N., van Heuven, S. M. a. C., Vandemark, D., Vlahos, P., Wallace, D. W. R., Wanninkhof, R. and Watson, A. J.: An update to the Surface Ocean CO₂ Atlas (SOCAT version 2), Earth Syst. Sci. Data, 6(1), 69–90, doi:<https://doi.org/10.5194/essd-6-69-2014>, 2014. [¶](#)

Beaufort Lagoon Ecosystems LTER and J. Kasper. 2020. Circulation dynamics: currents, waves, temperature measurements from moorings in lagoon sites along the Alaska Beaufort Sea coast, 2018-ongoing ver 2. Environmental Data Initiative. <https://doi.org/10.6073/pasta/3475cddb160a9f844aa5ede627c5f6fc> [¶](#)

Beaufort Lagoon Ecosystems LTER, Core Program. 2020. Photosynthetically active radiation (PAR) time series from lagoon sites along the Alaska Beaufort Sea coast, 2018-ongoing ver 1. Environmental Data Initiative. <https://doi.org/10.6073/pasta/ced2cedd430d430d9149b9d7f1919729> [¶](#)

Beaufort Lagoon Ecosystems LTER, Core Program. 2020. physicochemical water column parameters and hydrographic time series from river, lagoon, and open ocean sites along the Alaska Beaufort Sea coast, 2018-ongoing ver 1. Environmental Data Initiative. <https://doi.org/10.6073/pasta/e0e71c2d59bf7b08928061f546be6a9a> [¶](#)

Beaufort Lagoon Ecosystems LTER, Core Program. 2020. Time series of water column pH from lagoon sites along the Alaska Beaufort Sea coast, 2018-ongoing ver 1. Environmental Data Initiative. <https://doi.org/10.6073/pasta/9305328d0f1ed28fbb2d7cf56c686786> [¶](#)

Bresnahan, P. J., Martz, T. R., Takeshita, Y., Johnson, K. S. and LaShomb, M.: Best practices for autonomous ... [11]

Deleted: [¶](#)

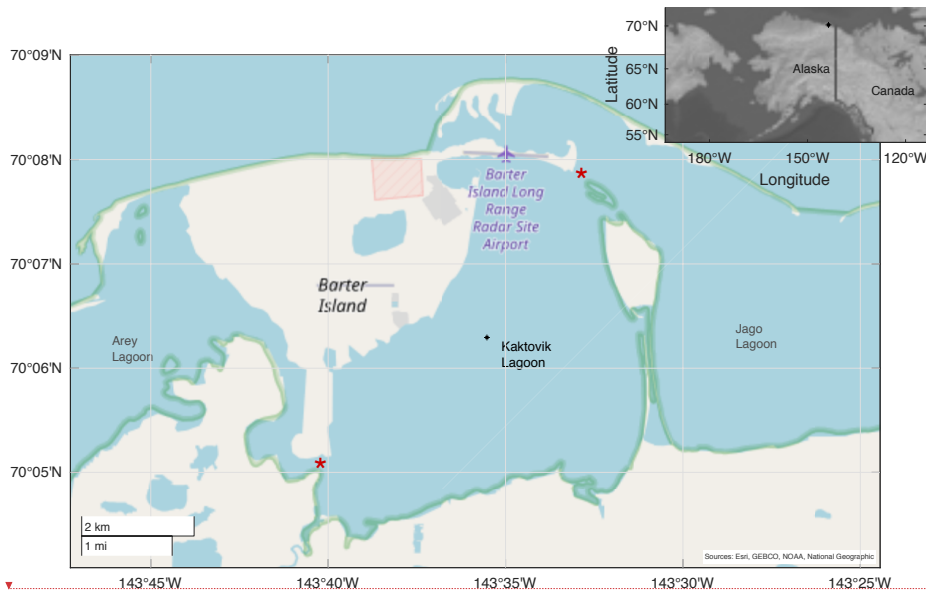
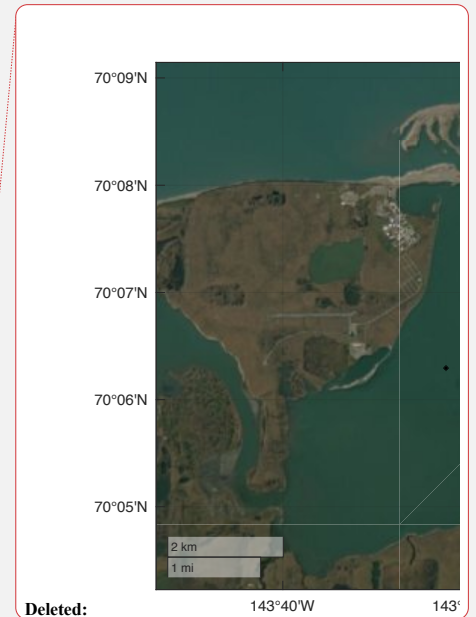


Figure 1. Study site at Kaktovik Lagoon along the Beaufort Sea Coastline. Red stars denote the main exchange pathways between adjacent lagoons and greater Beaufort Sea. Black star in inset map is location of Kaktovik Lagoon.



1393

1394

1395

1396

1397

1398

1399

1400

1401

1402

1403

1404

1405

1406

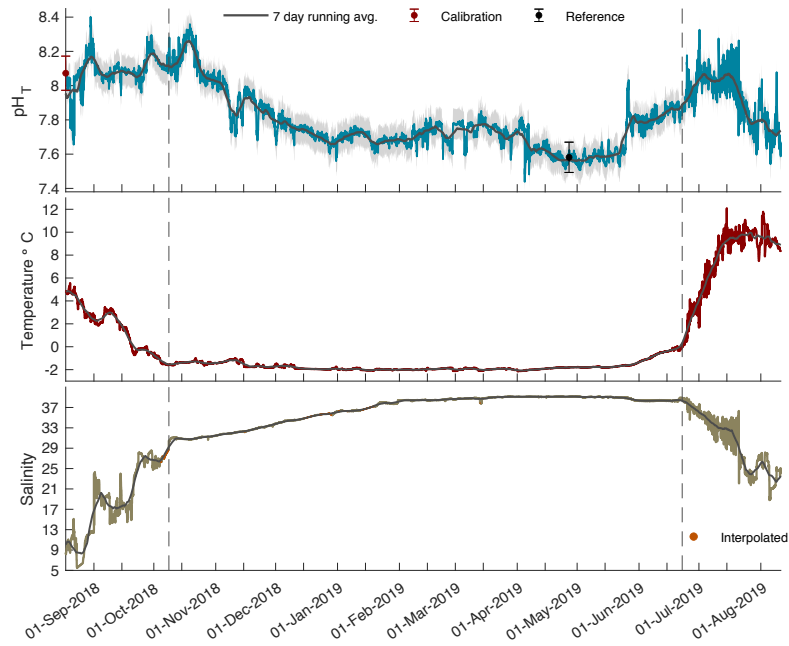
1407

1408

1409

1410

1411



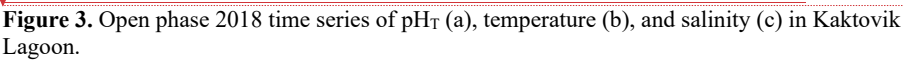
a.

b.

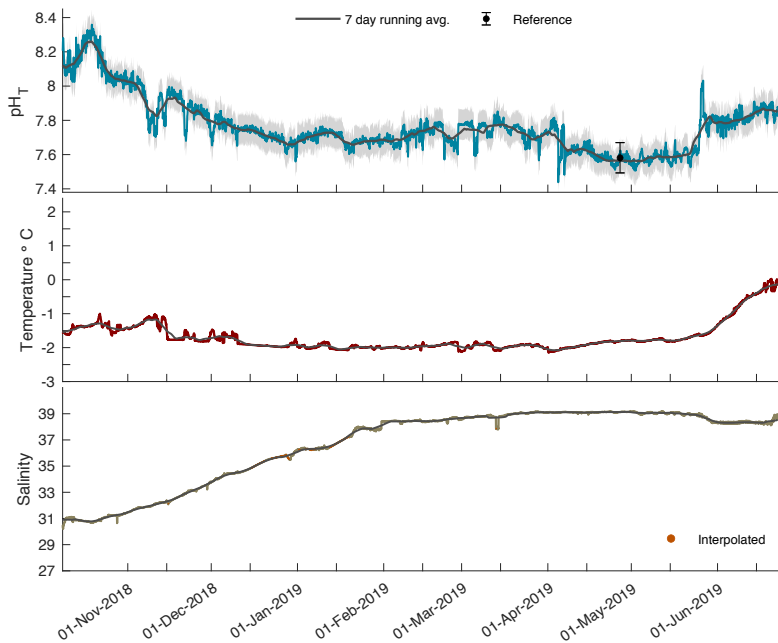
c.

Figure 2. Times series of pH_T (a), temperature (b), and salinity (c) in Kaktovik Lagoon for entire deployment period from 17 August 2018 to 11 August 2019. The first section to the left of the dashed line is open phase 2018, the middle section is closed 2018 – 2019, and the last section to the right of the second dashed line is open phase 2019.

1416
1417
1418
1419
1420
1421
1422
1423
1424
1425
1426
1427
1428
1429
1430
1431
1432
1433
1434
1435



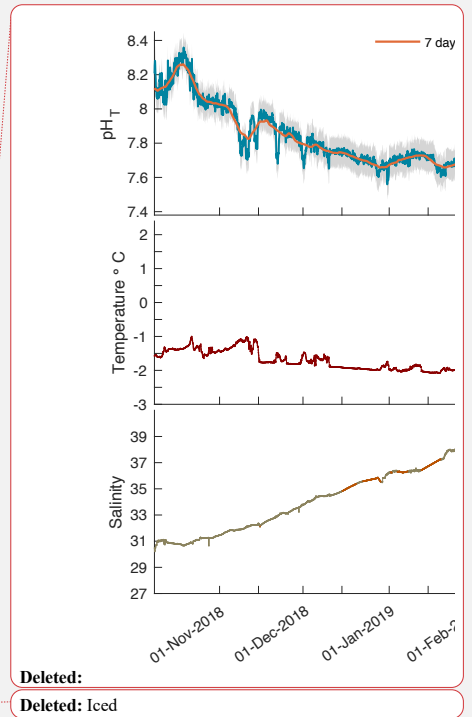
1437
1438
1439



1440
1441
1442
1443
1444
1445
1446
1447
1448
1449
1450
1451
1452
1453
1454
1455
1456
1457
1458
1459

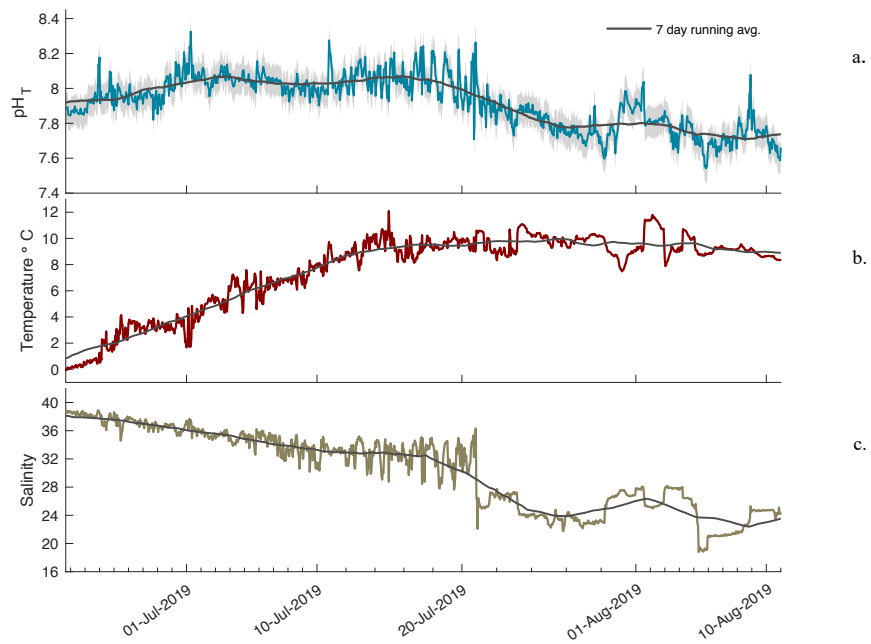
Figure 4. Closed phase 2018 – 2019 time series of pH_T (a), temperature (b), and salinity (c) in Kaktovik Lagoon.

a.
b.
c.

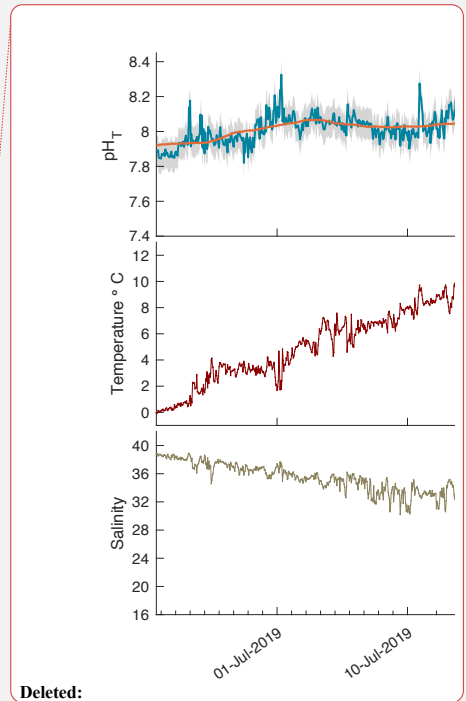


Deleted:
Deleted: Iced

1462
1463
1464



1465
1466 **Figure 5.** Open phase 2019 time series of pH_T (a), temperature (b), and salinity (c) in Kaktovik
1467 Lagoon.
1468
1469
1470
1471
1472
1473
1474
1475
1476
1477
1478
1479
1480
1481
1482



Deleted:

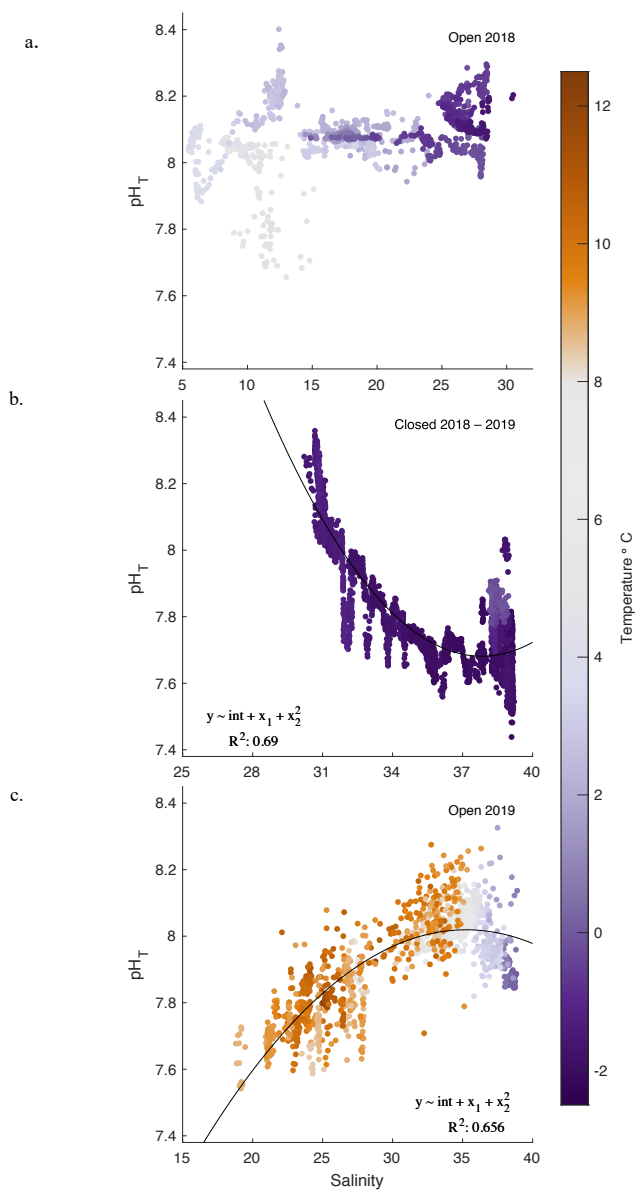


Figure 6. pH_T-salinity correlations for open 2018 (a), Closed 2018 – 2019 (b), and open 2019 (c). Quadratic fits are applied to iced and open 2019 phases only. Temperature is represented in color for all correlations.

Deleted: iced

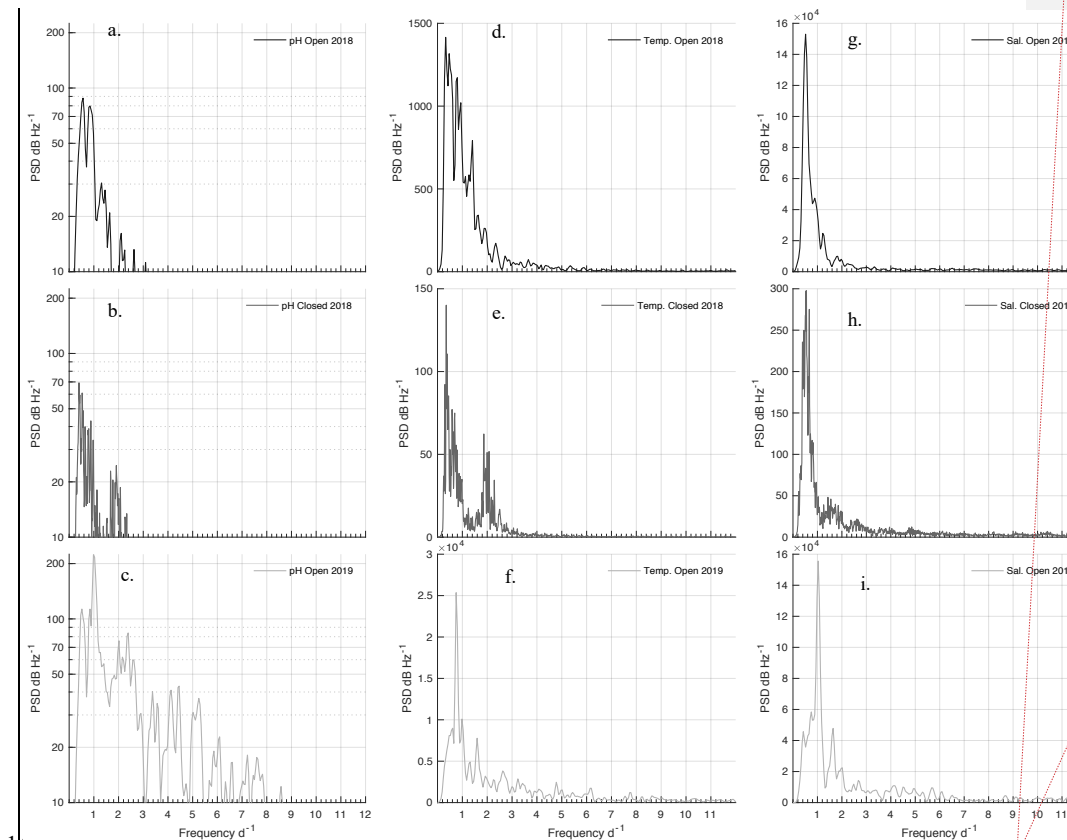
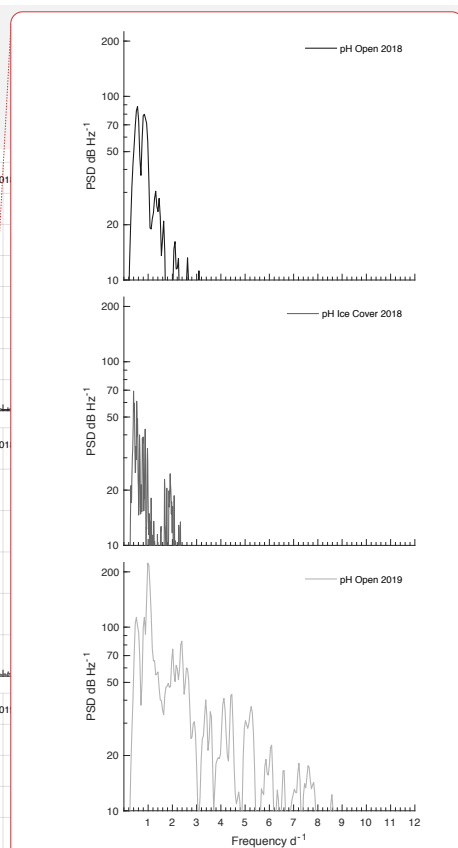
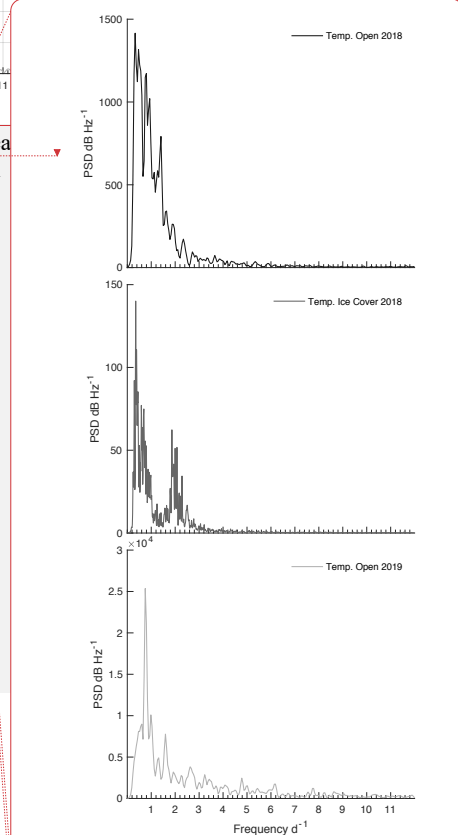


Figure 7. Power Spectral Density (PSD) plots for pH_T (a,b,c), temperature (d,e,f), and salinity (g,h,i) at ea phase of the time series: open 2018 (top row), Closed 2018 – 2019 (middle row), and open 2019 (bottom row).



deleted:



deleted:

deleted: ph

Deleted: ice-cover

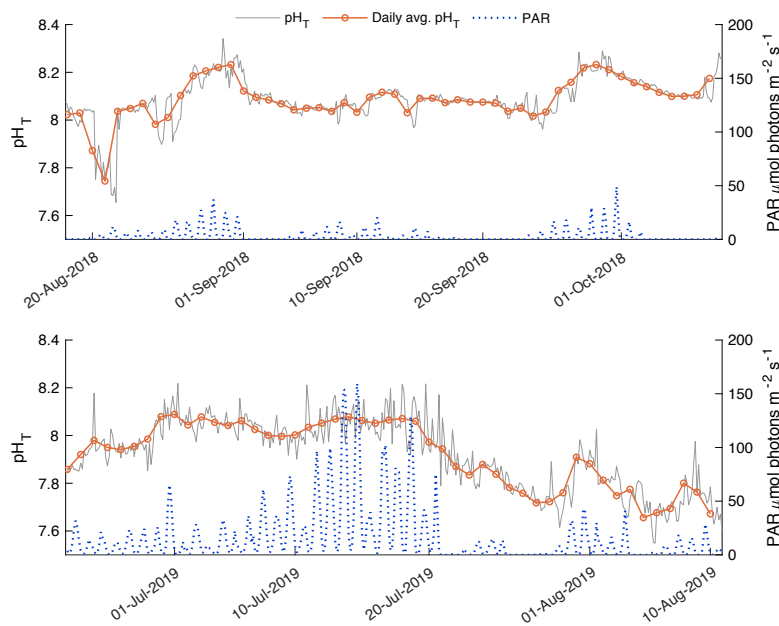
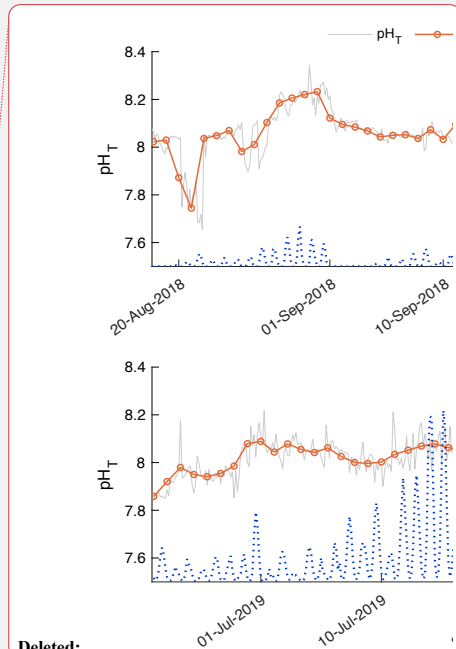


Figure 8. Detrended pH_T (gray line) and PAR (blue dots) for open phase 2018 (a) and open phase 2019 (b). Daily average pH_T (orange line) is displayed overtop hourly variability.



Deleted:

Deleted: ¶

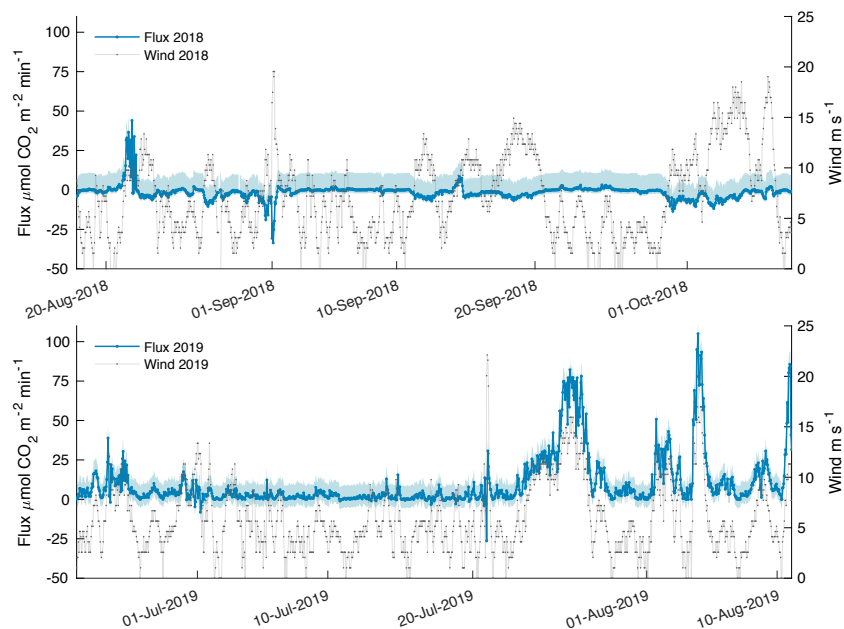


Figure 9. Estimated carbon flux (orange) and wind speed (grey) for open phase 2018 (a) and open

phase 2019 (b). Estimated flux potential is shaded in blue where the upper bound is associated with

Deleted: Uncertainty around each estimate

difference in PCO₂ from the A_T-salinity_{in situ} regression, and the lower bound associated with

freshwater Schmidt number. The upper and lower bounds for

Deleted: Schmidt

open 2018 were 10.67 and 2.23 $\mu\text{mol C m}^{-2} \text{ min}^{-1}$ while open 2019 upper and lower bounds were 8.56

and 5.52 $\mu\text{mol C m}^{-2} \text{ min}^{-1}$, respectively.

Page 42: [1] Deleted	Cale Miller	12/11/20 1:12:00 PM
----------------------	-------------	---------------------

Page 49: [2] Deleted	Cale Miller	12/15/20 3:56:00 PM
----------------------	-------------	---------------------